The formation of rings and gaps in wind-launching, non-ideal MHD disks

Scott Suriano (UTokyo)

Great Barriers in Planet Formation

Palm Cove, Queensland, Australia

22 July 2019

magnetic island

Magnetic Island

Queensland
Australia

4.4 ★★★★★ (99)

Island

Directions | Save | Nearby | Send to your phone | Share

Queensland, Australia

Add a label

Photos

Magnetic Island

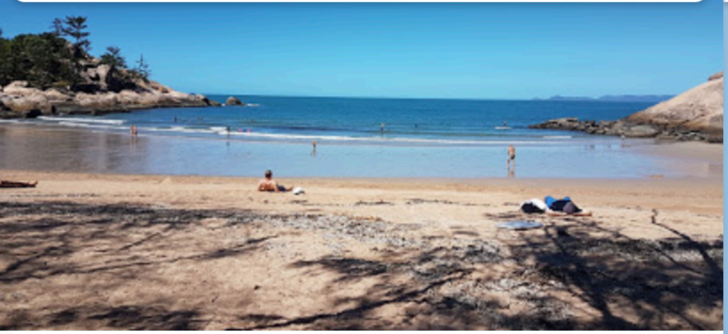

Alma Bay

4.7 ★★★★★ (346)

Tourist attraction

Directions · Save · Nearby · Send to your phone · Share

Magnetic Island, LOT 156 Armand Way, Magnetic Island QLD 4819, Australia

VV29+MC Arcadia, Queensland, Australia

nprsr.qld.gov.au

Open now: Open 24 hours

Claim this business

Add a label

Suggest an edit

Add missing information

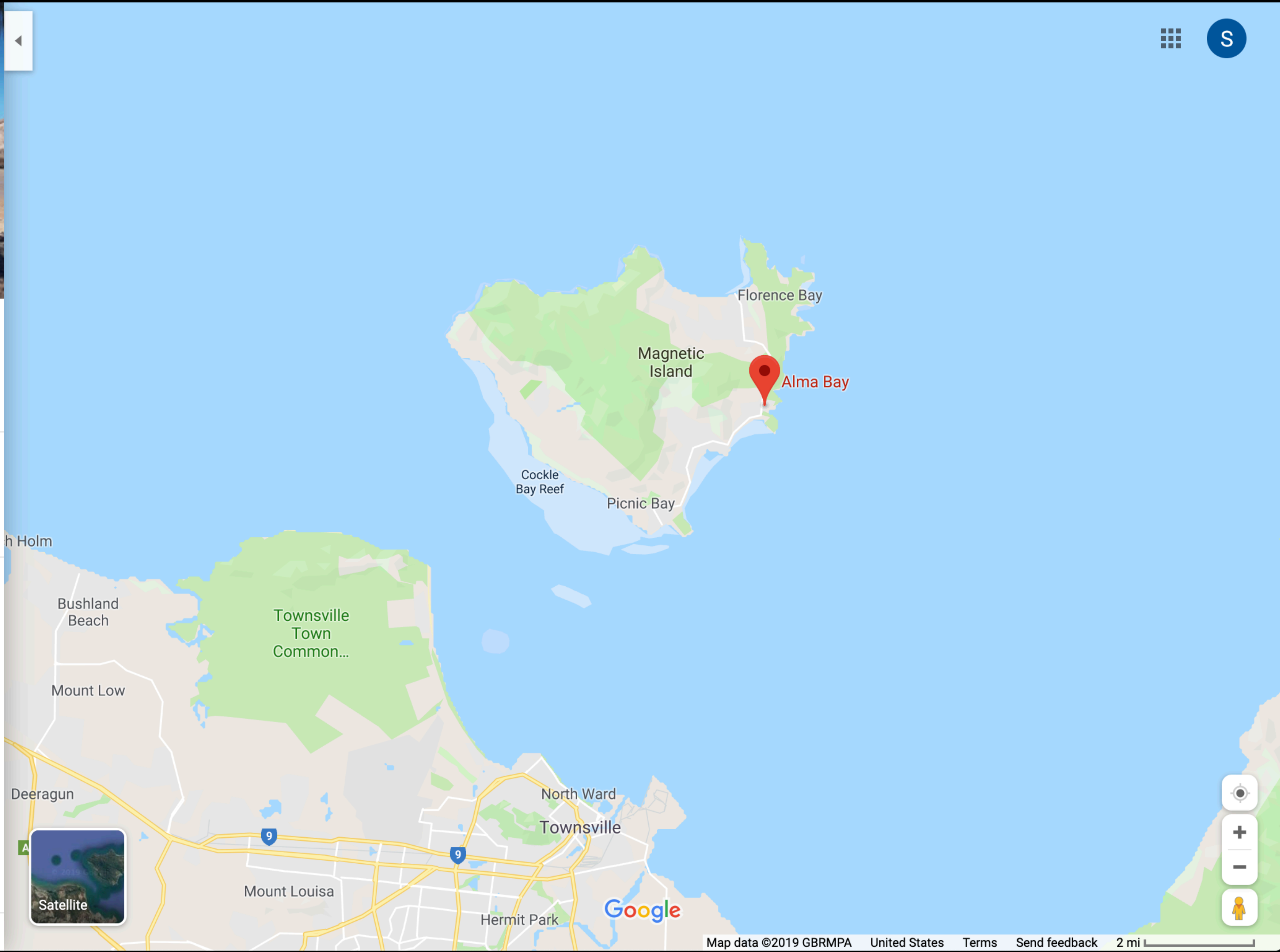

Magnetic Island

Alma Bay

4.7 ★★★★★ (346)

Tourist attraction

Directions

Save

Nearby

Send to your phone

Share

Magnetic Island, LOT 156 Armand Way, Magnetic Island QLD 4819, Australia

VV29+MC Arcadia, Queensland, Australia

nprsr.qld.gov.au

Open now: Open 24 hours

Claim this business

Add a label

Suggest an edit

Add missing information

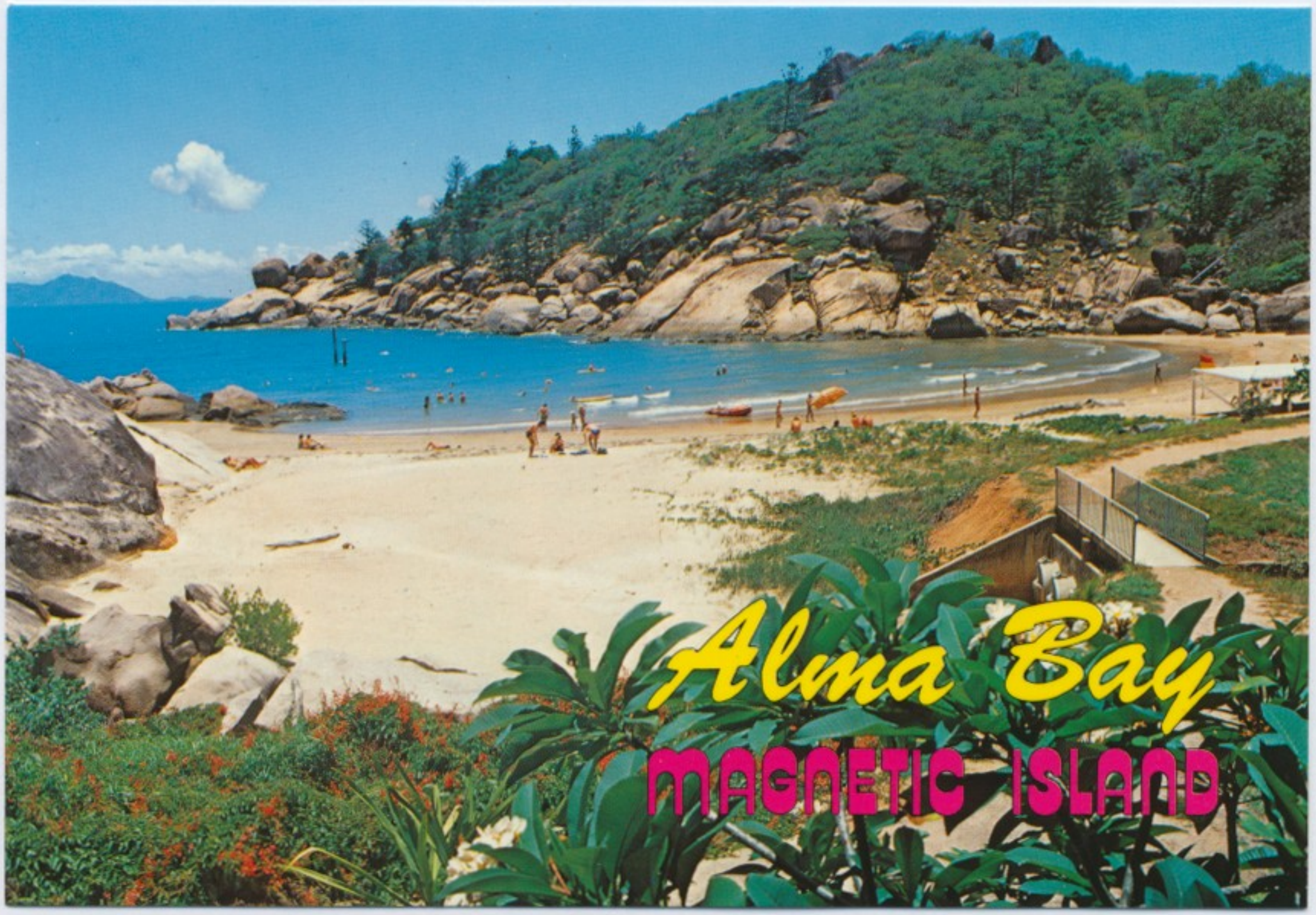

ALMA Large Program DSHARP

Disk substructure is common!

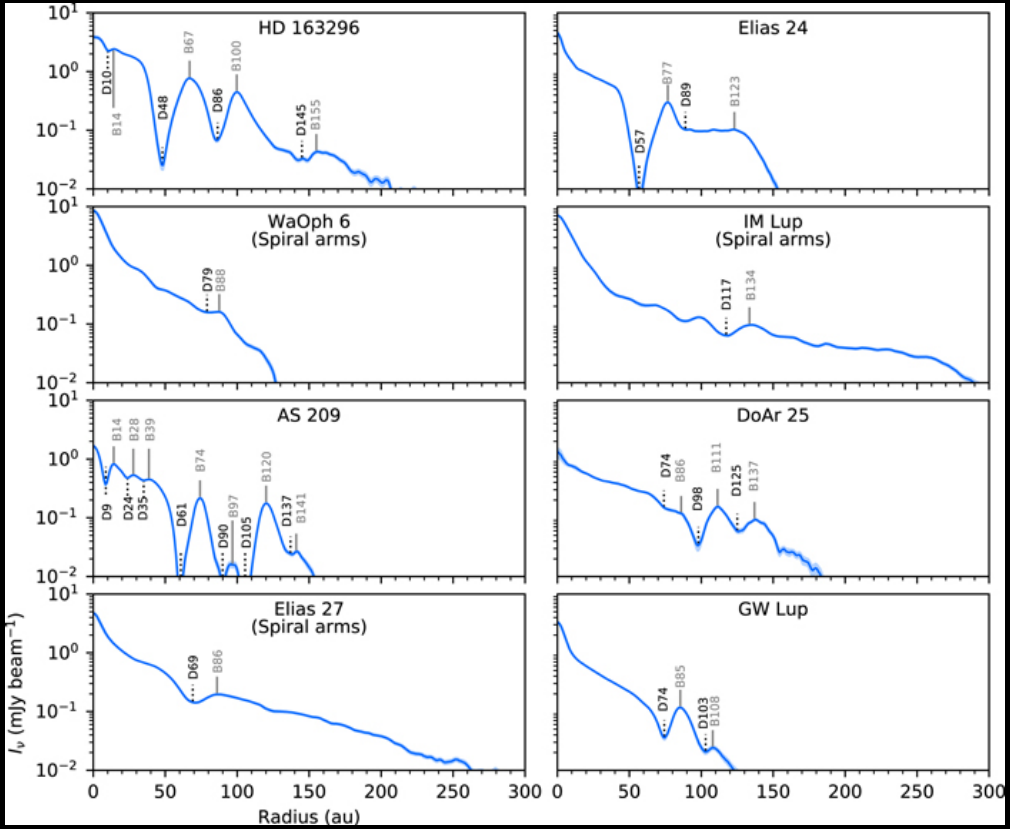

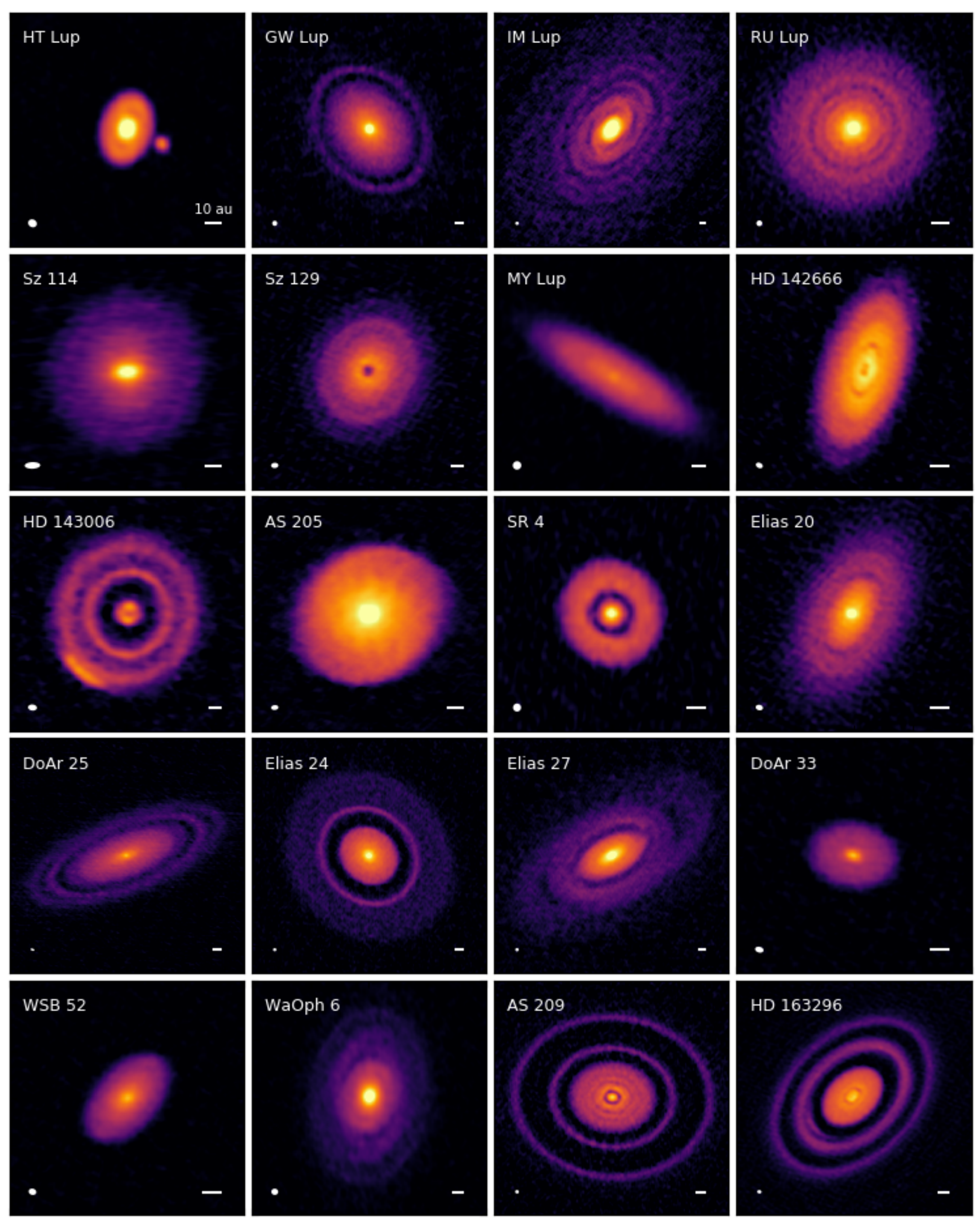

Andrews+ *2018*

https://almascience.nao.ac.jp/almadata/lp/DSHARP/

Disk Substructure Formation Mechanisms

1. Gap clearing by planets (Dong+ 2015, 2017; Bae+ 2017; etc.)
2. Rapid pebble growth at the condensation fronts of major volatiles (Zhang+ 2016; Andrews+ 2016)
3. Pile up of volatile ices in sintering zones outside of snow lines (Okuzumi+2016)
4. Secular gravitational instability (Takahashi & Inutsuka 2014, 2016)
5. Changes in the disk viscosity at the edge of MRI dead zone (Flock+ 2015; Ruge+ 2016)
6. Zonal flows and magnetic self-organization (Bethune+2017; Riols & Lesur 2018; Krapp+2018)
7. Magnetic disk winds (Suriano+ 2017, 2018, 2019; Takahashi & Muto 2018; Hu+ 2019; see Riols & Lesur 2019 for treatment of linear wind instability; see also "clump/stripe" instability of Moll 2012)

Observational evidence for disk winds: Resolved images of extended disk wind

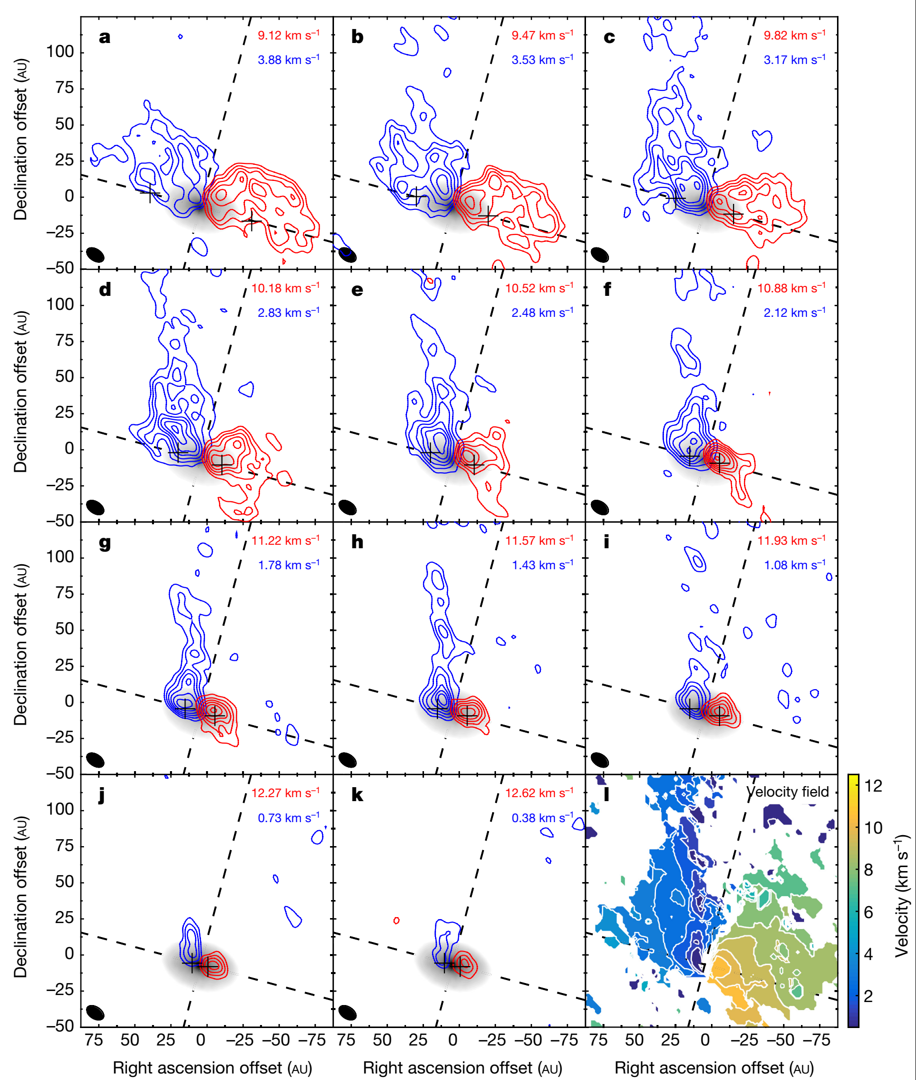

ALMA observations of CO in TMC1A show launching radii from 1 – 20 au

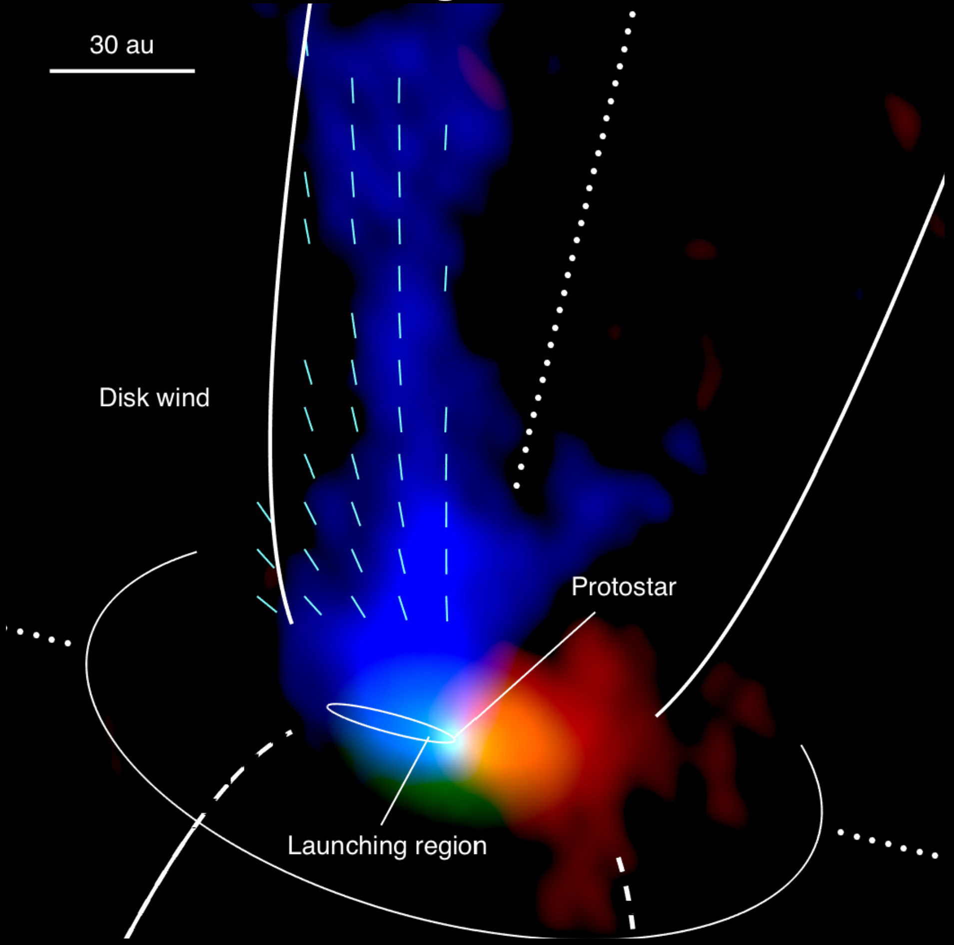

Bjerkeli+16

Observational evidence for disk winds: SiO outflow from massive Orion Source I

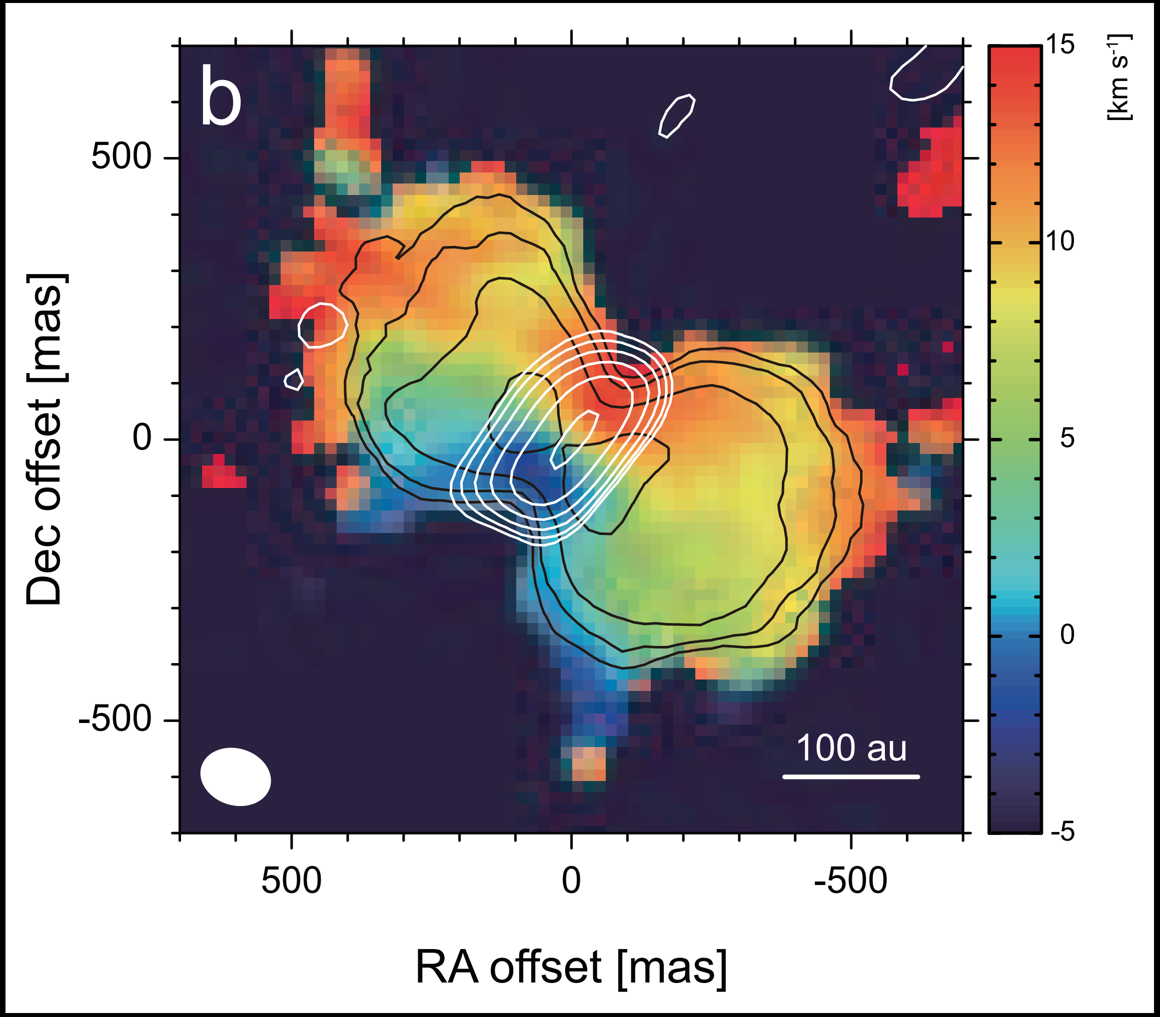

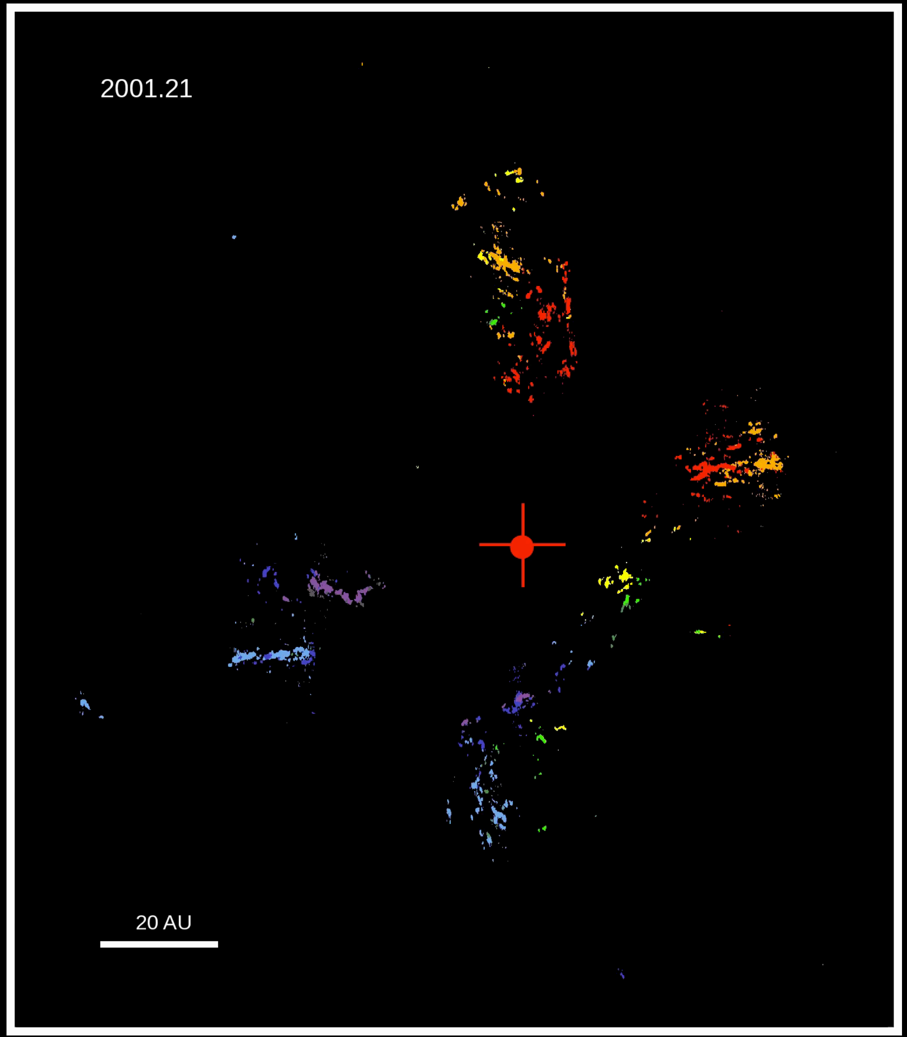

Hirota+17

Matthews+10

Observational evidence for disk winds: optical forbidden line emission

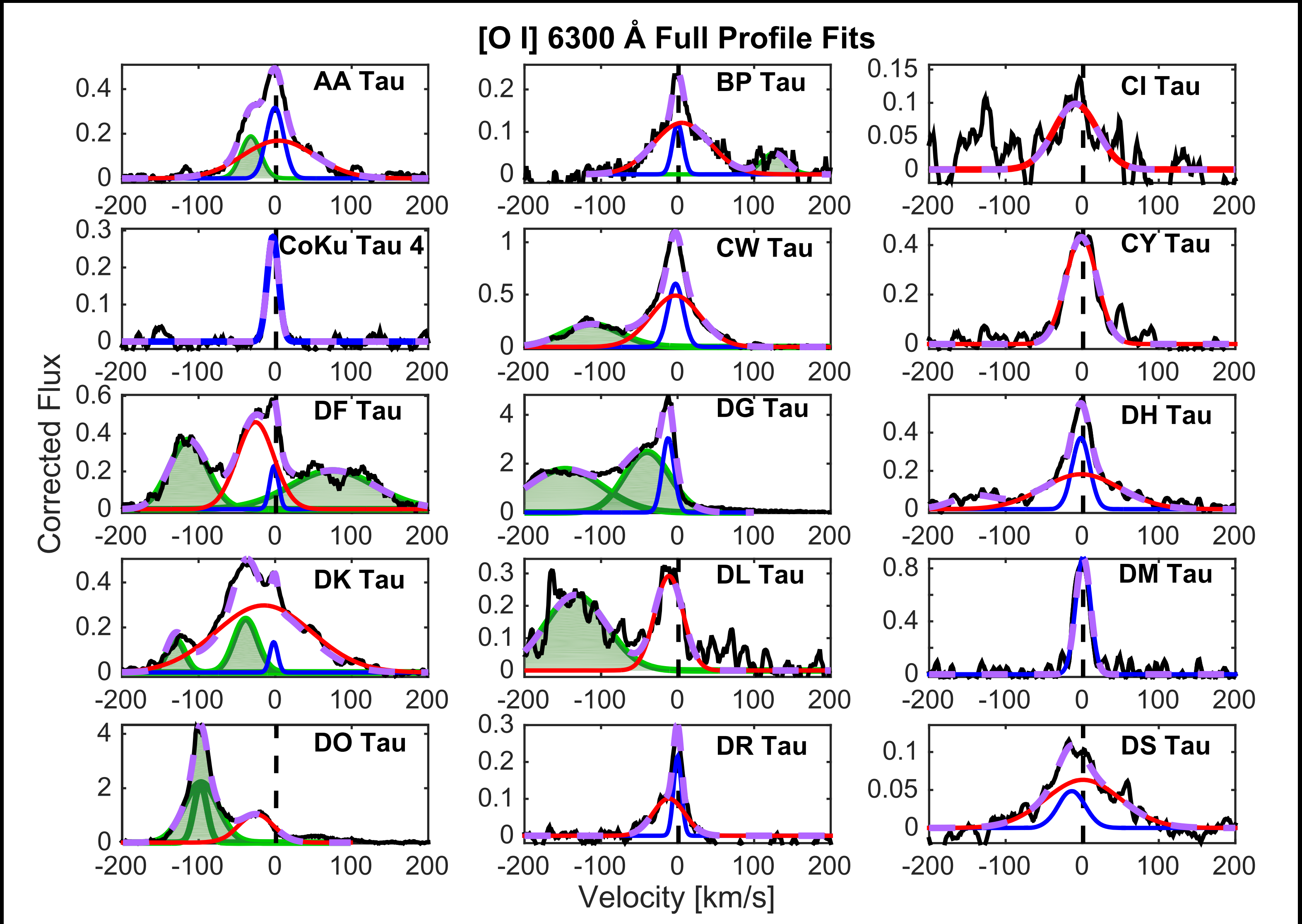

Simon+ 2016
(also Fang+ 2018,
Banzatti+ 2019)

The magnetocentrifugal wind (MCW)

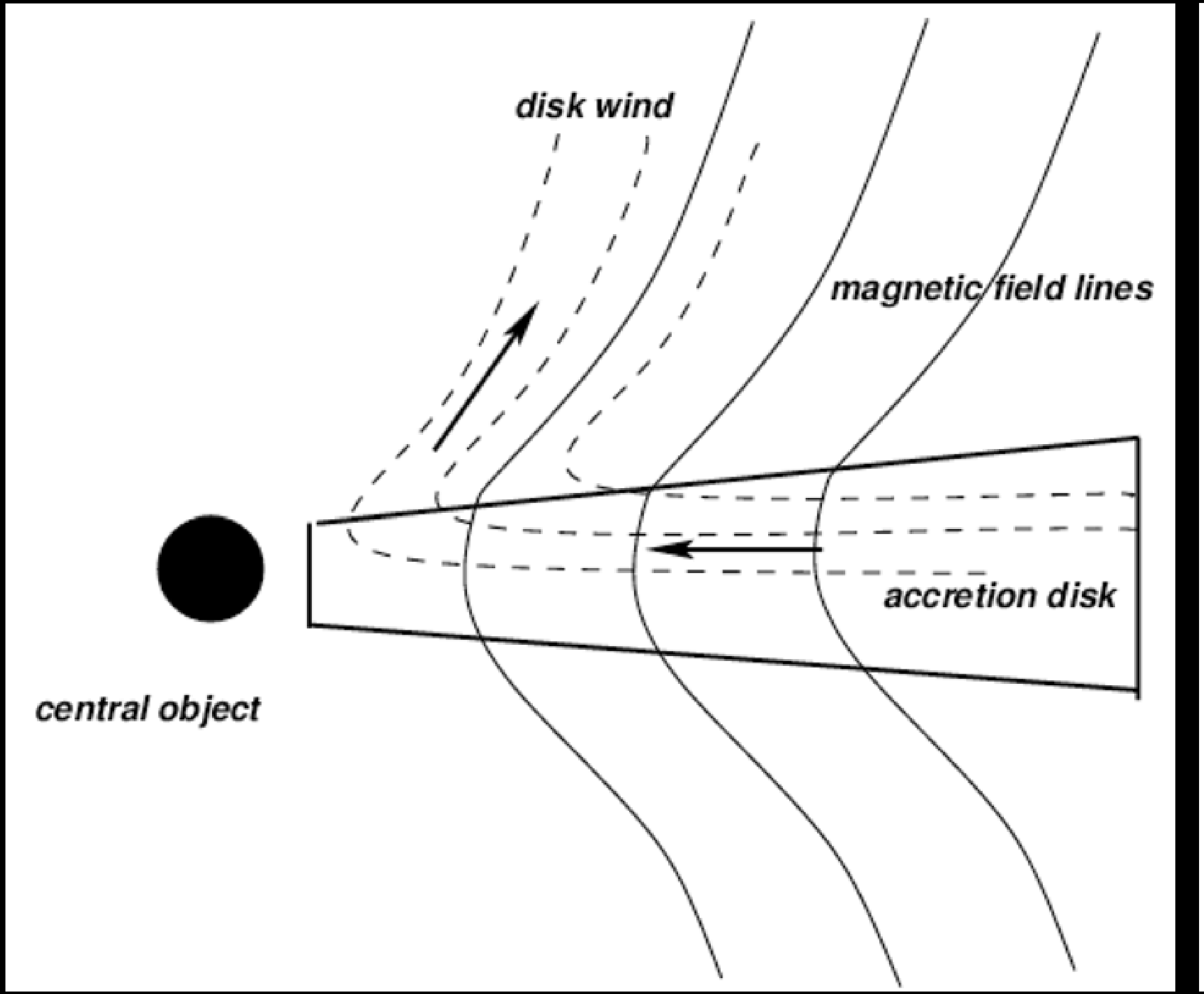

Sheikhnezami+ 2012

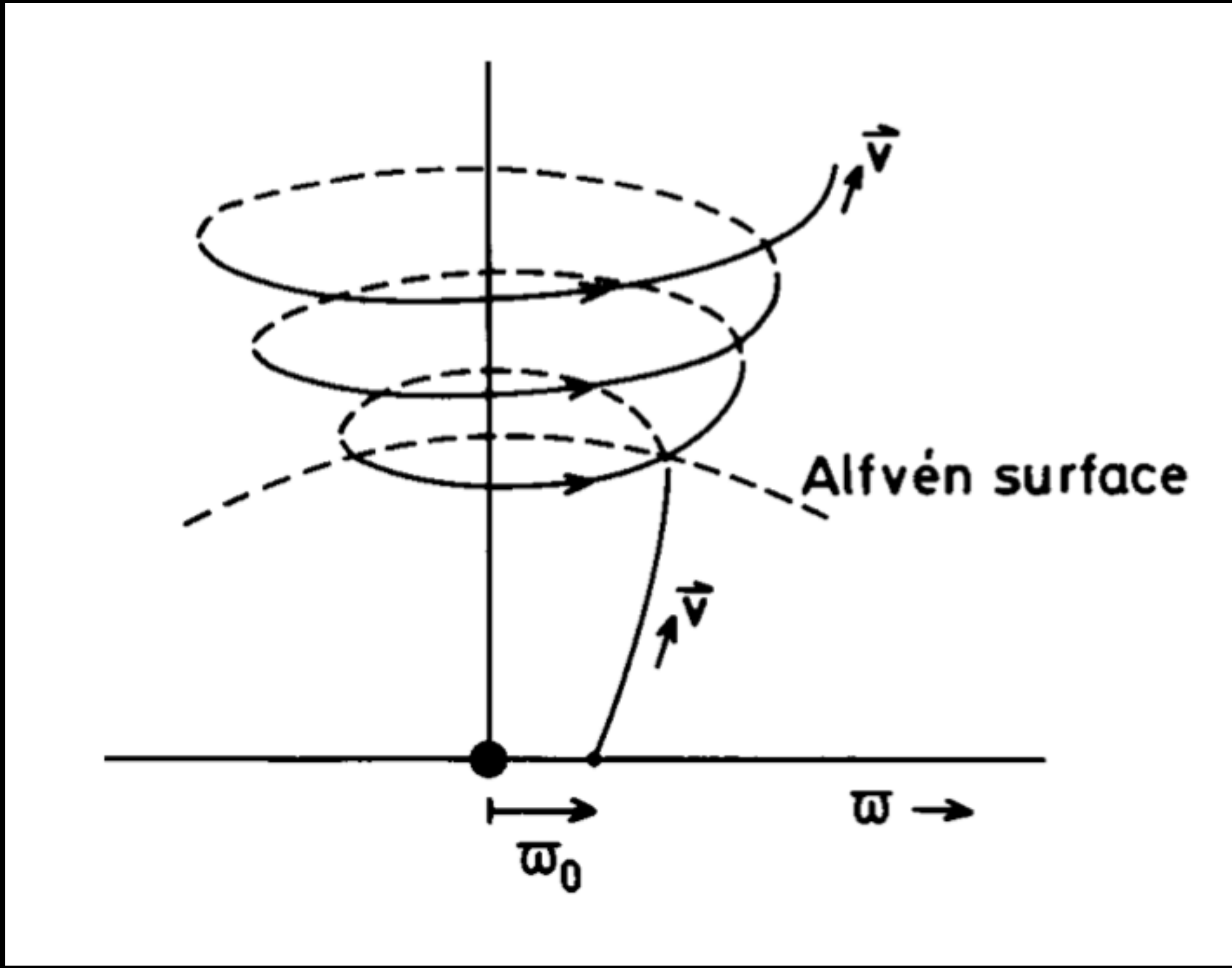

Spruit 2009

Magnetic coupling regimes

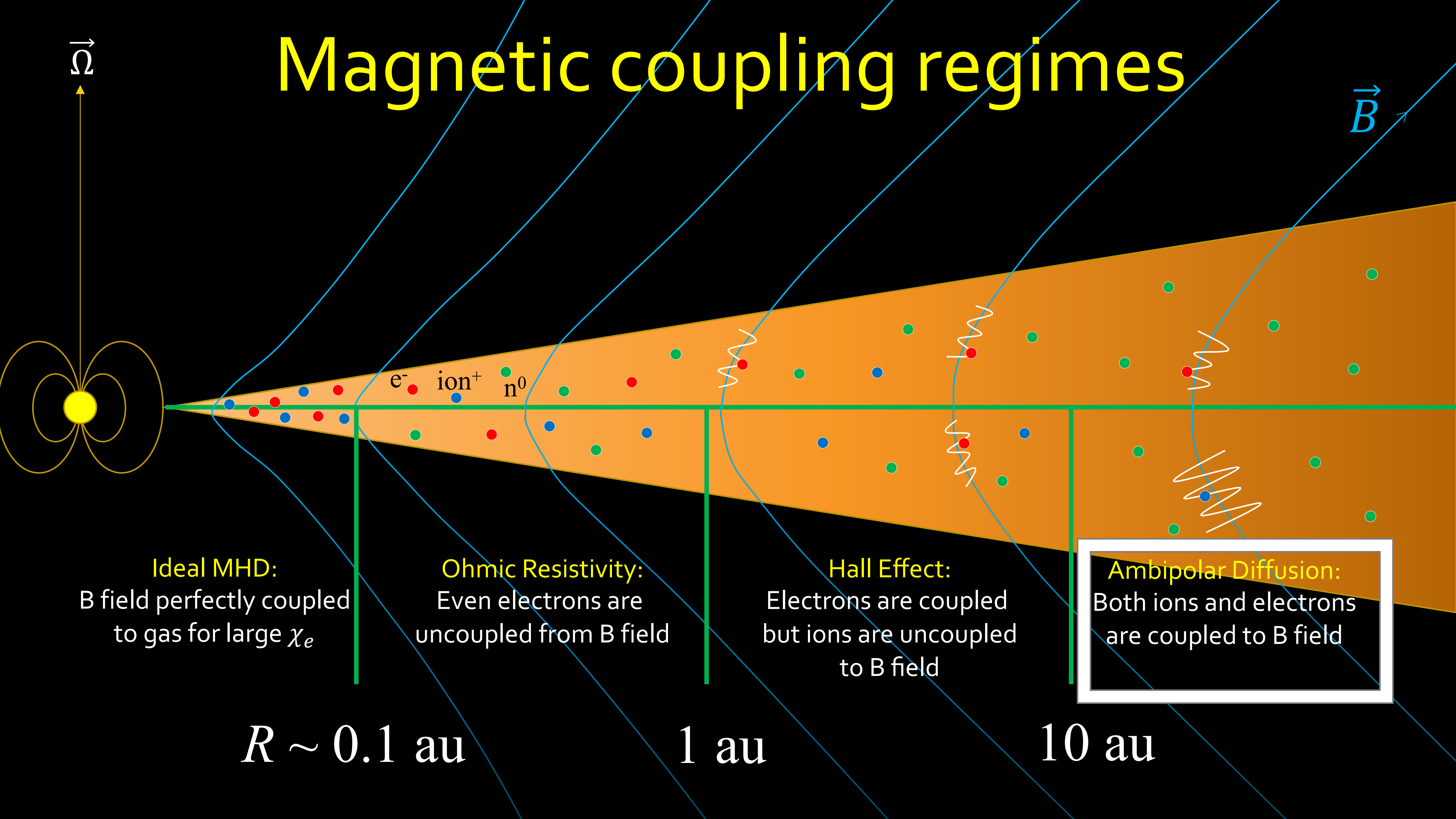

Simulation setup

- ZeusTW grid based code in spherical polar coordinates
- Axisymmetric (includes phi vector components)
- Non-rotating, hydrostatic corona above disk with pressure balanced at disk surface
- *Ambipolar diffusion* where $\rho_{\mathrm{ion}} \propto \rho^{1/2}$ with transition to ideal MHD above disk surface

$$\frac{\partial \rho}{\partial t} + \nabla \cdot (\rho \boldsymbol{v}) = 0,$$

$$\rho \frac{\partial \boldsymbol{v}}{\partial t} + \rho\,(\boldsymbol{v} \cdot \nabla)\,\boldsymbol{v} = -\nabla P + \boldsymbol{J} \times \boldsymbol{B}/c - \rho \nabla \Phi_g,$$

$$\boldsymbol{J} = (c/4\pi) \nabla \times \boldsymbol{B}$$

$$\frac{\partial \boldsymbol{B}}{\partial t} = \nabla \times (\boldsymbol{v} \times \boldsymbol{B}) - \frac{4\pi}{c} \nabla \times (\eta_A \boldsymbol{J}_\perp)\,, \quad \eta_A = \frac{B^2}{4\pi \gamma_i \rho \rho_i}$$

$$\boldsymbol{J}_\perp = -\boldsymbol{J} \times \boldsymbol{B} \times \boldsymbol{B}/B^2$$

$$\frac{\partial e}{\partial t} + \nabla \cdot (e \boldsymbol{v}) = -P \nabla \cdot \boldsymbol{v}, \quad P = (\gamma - 1) e$$

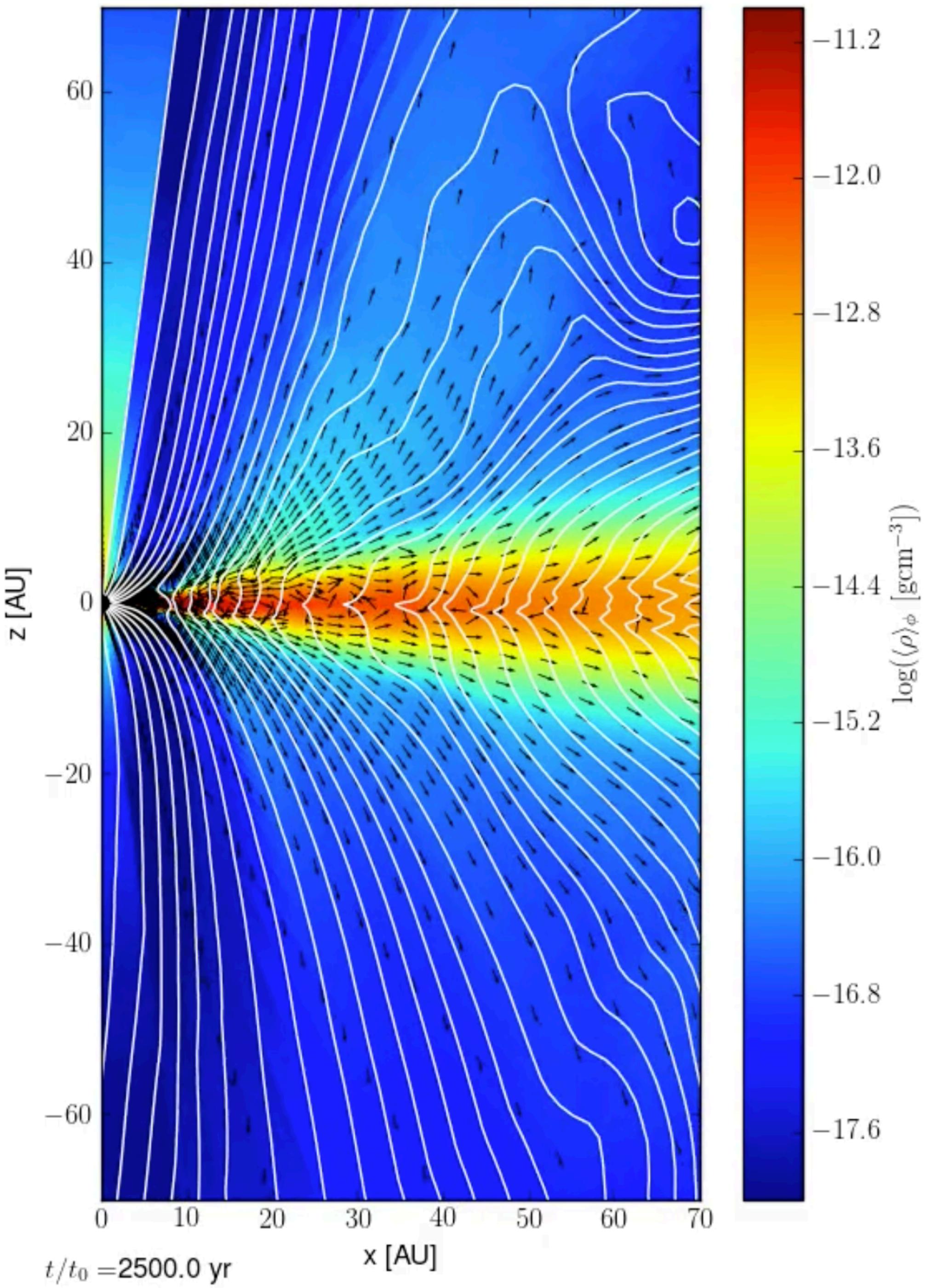

Simulation results

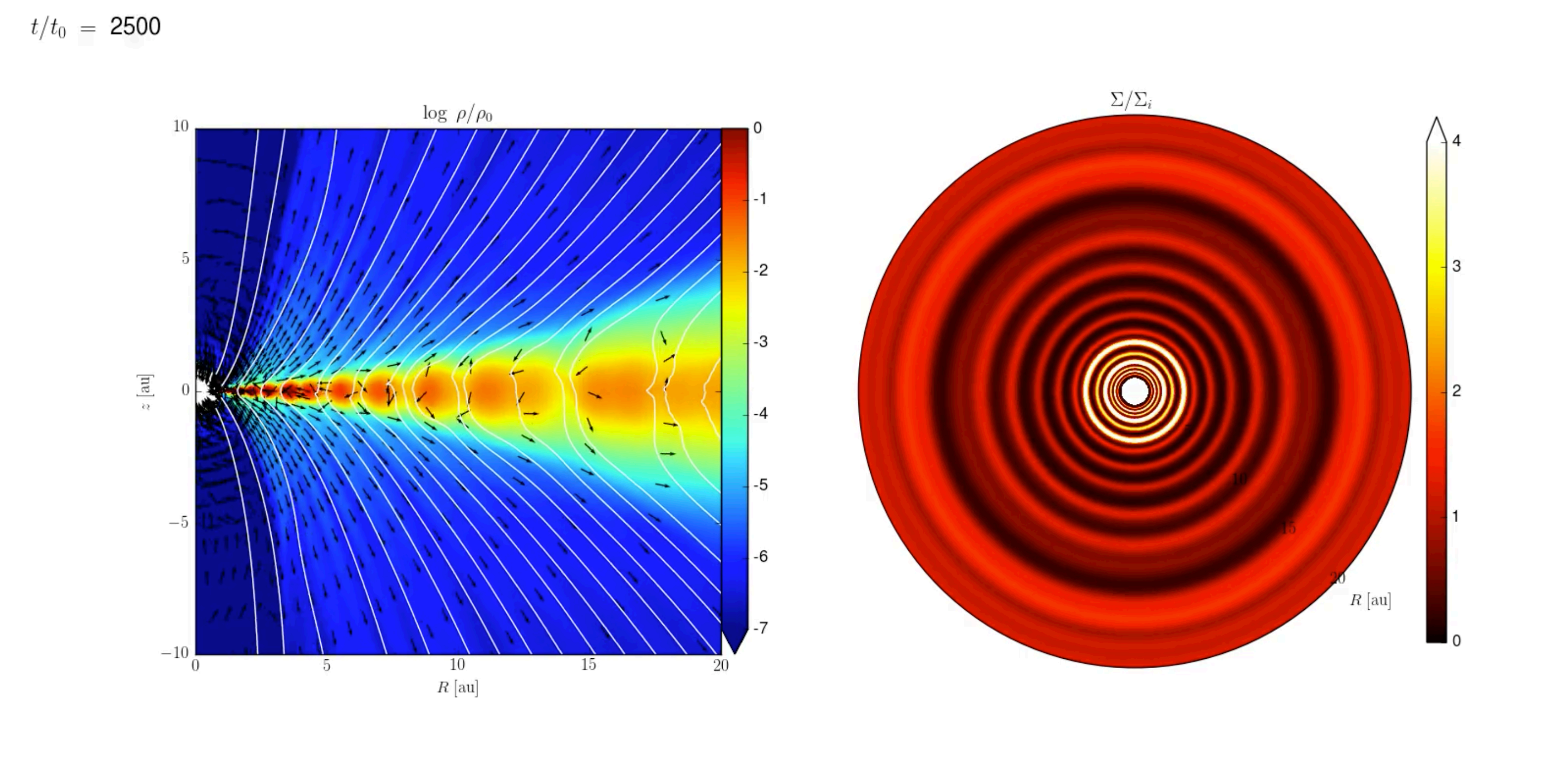

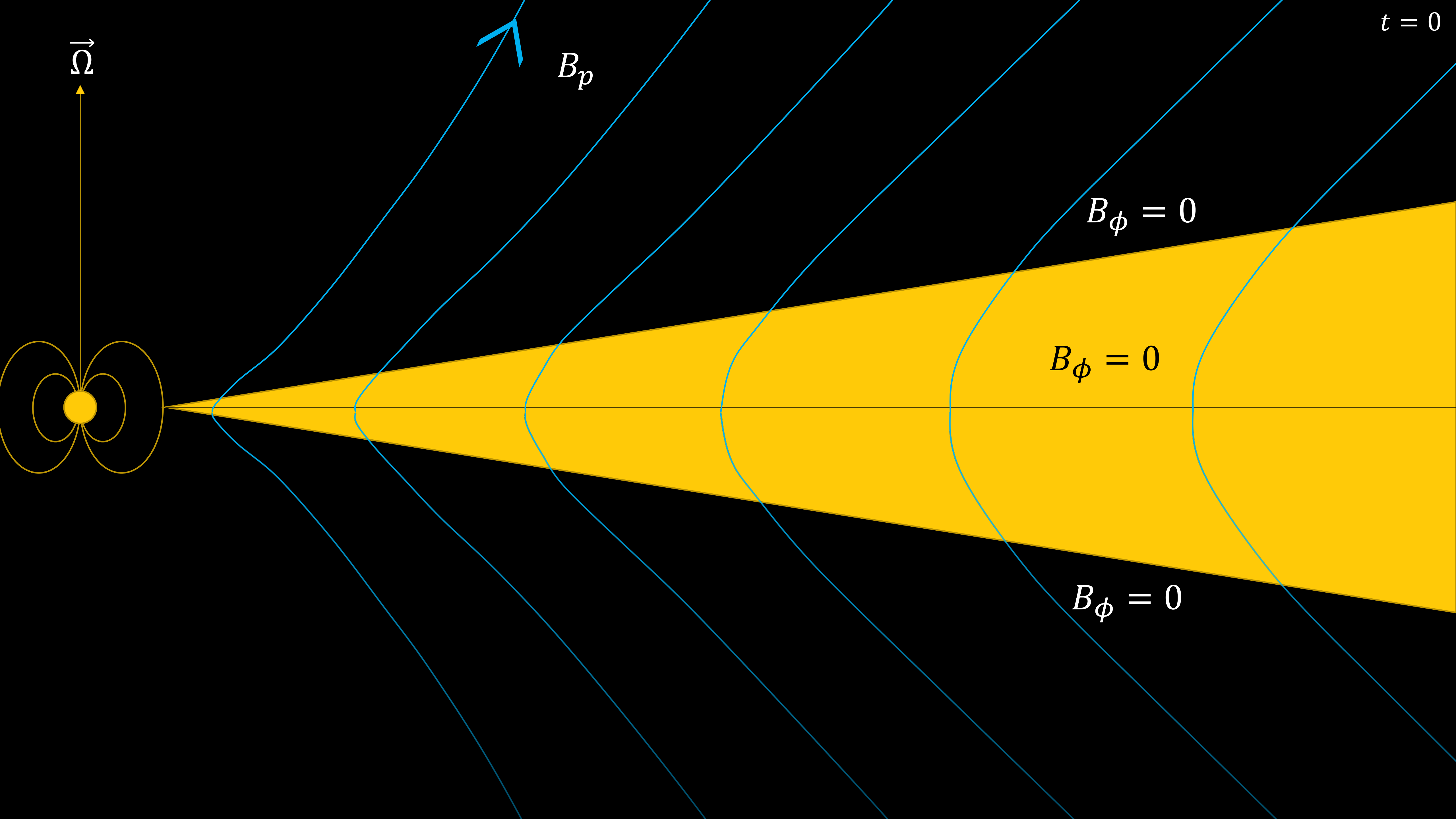

$t = 0$
$\vec{\Omega}$
B_p
$B_\phi = 0$
$B_\phi = 0$
$B_\phi = 0$

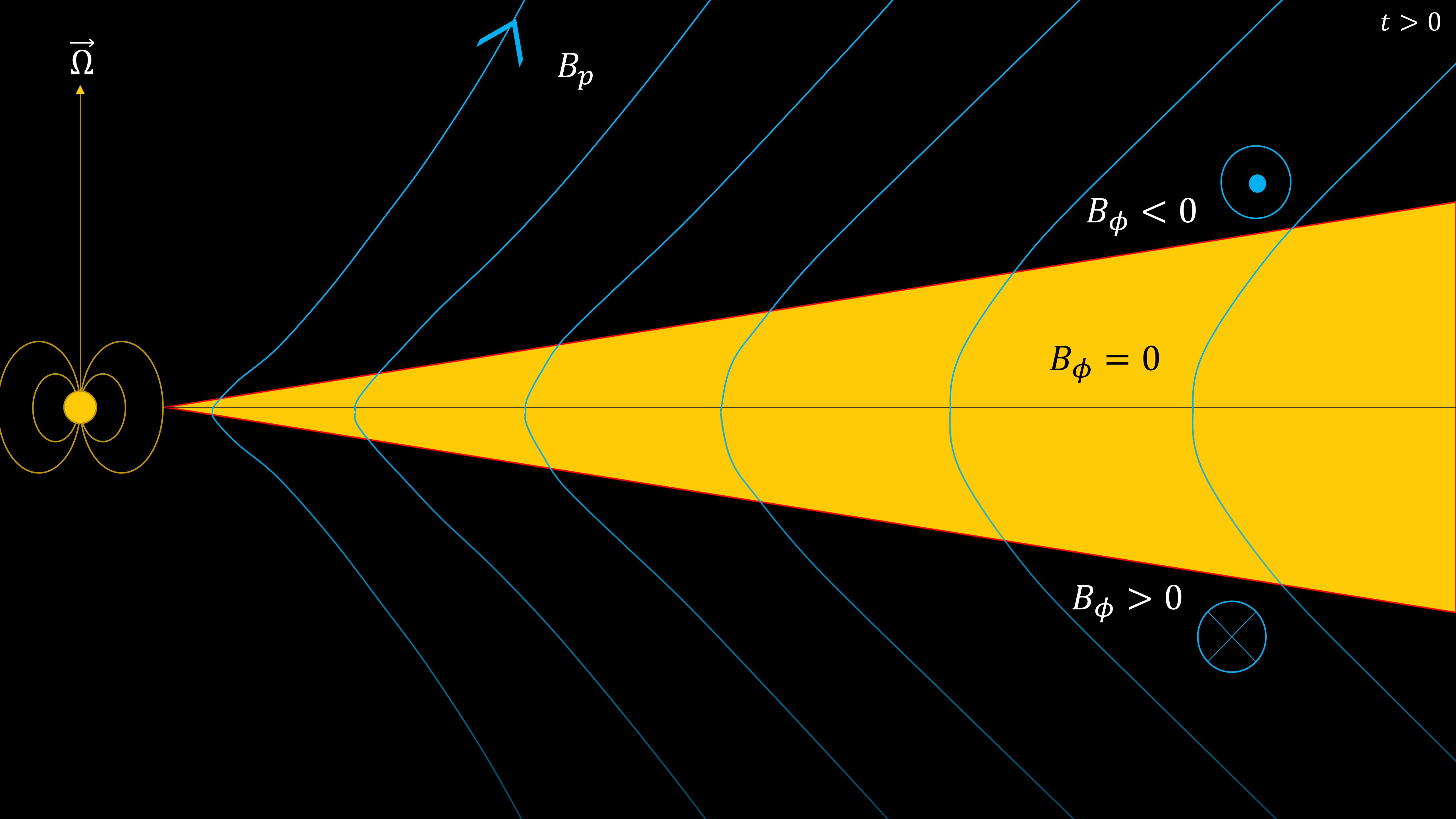

$t > 0$
$\vec{\Omega}$
B_p
$B_\phi < 0$
$B_\phi = 0$
$B_\phi > 0$

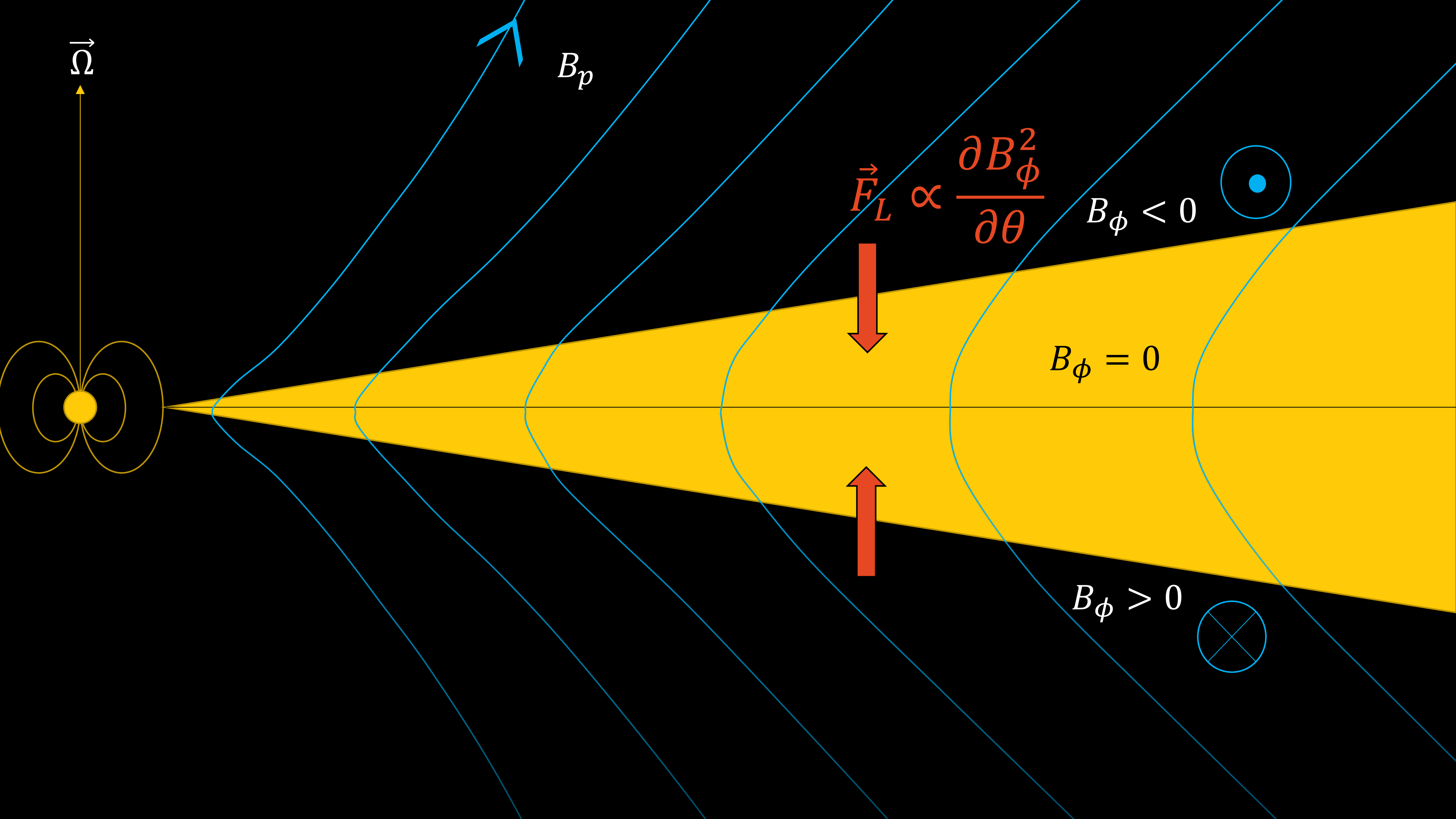

$\vec{\Omega}$
B_p
$\vec{F}_L \propto \frac{\partial B_\phi^2}{\partial \theta}$
$B_\phi < 0$
$B_\phi = 0$
$B_\phi > 0$

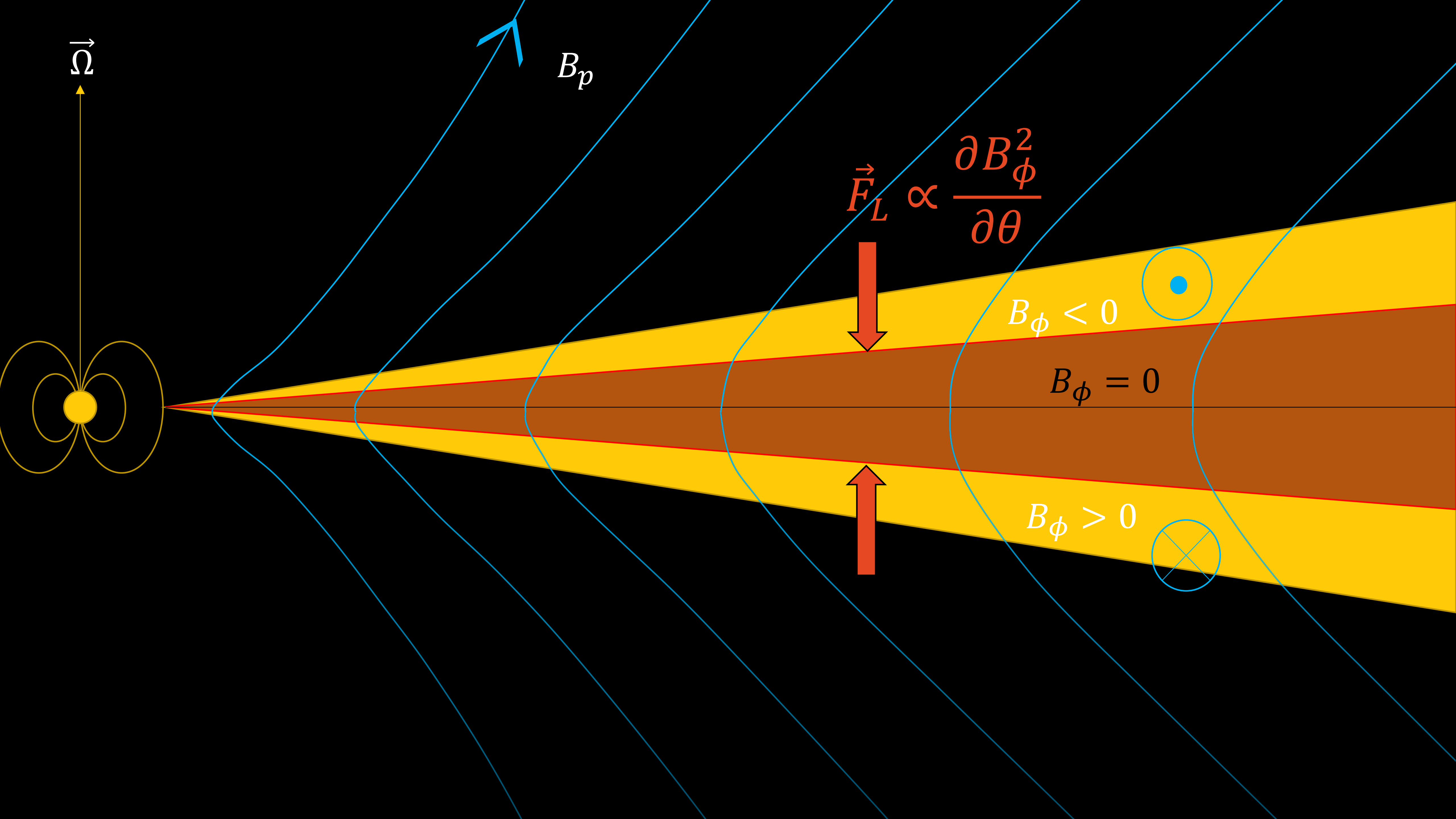

$\vec{\Omega}$
B_p
$\vec{F}_L \propto \frac{\partial B_\phi^2}{\partial \theta}$
$B_\phi < 0$
$B_\phi = 0$
$B_\phi > 0$

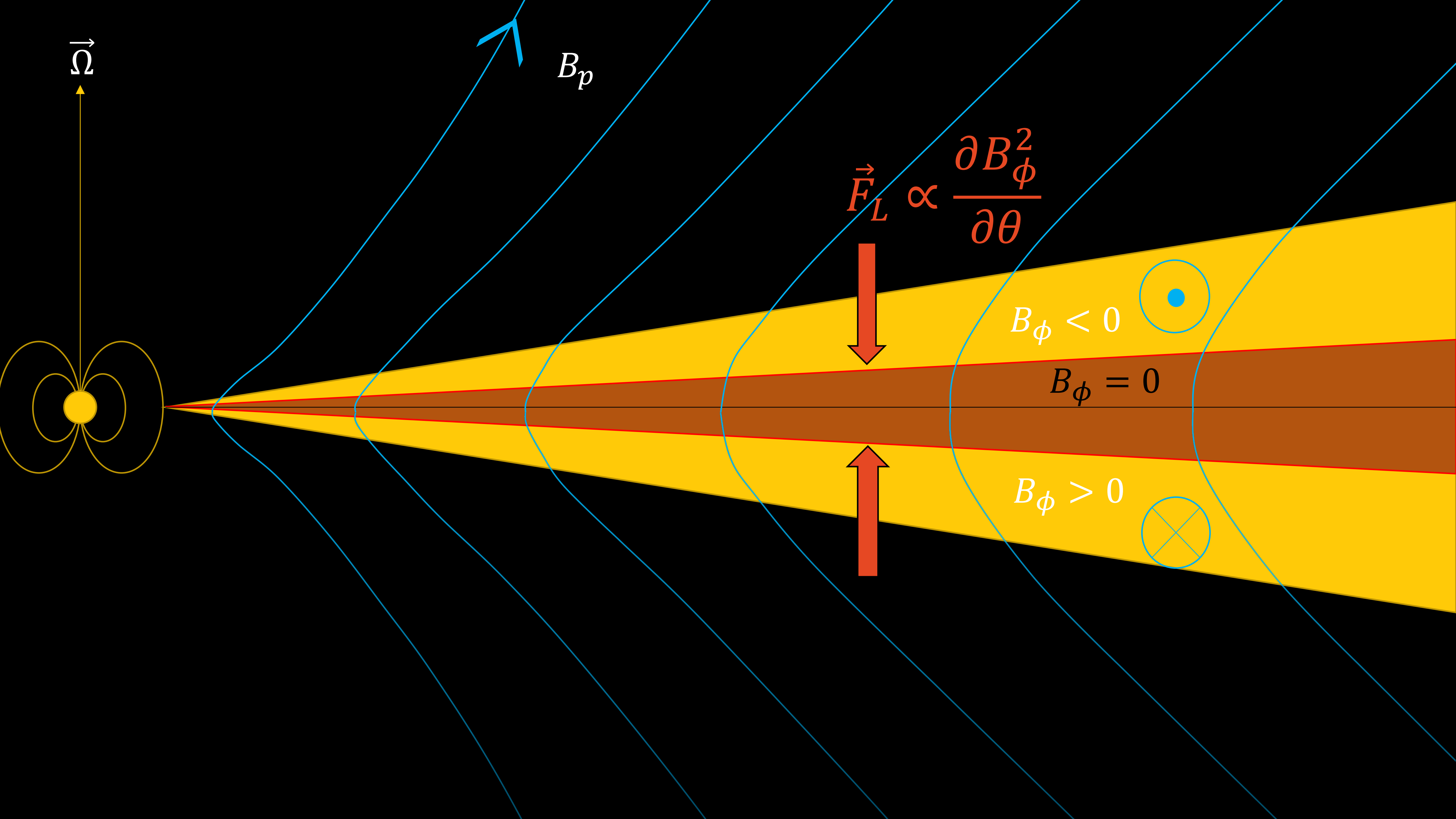

$\vec{\Omega}$
B_p
$\vec{F}_L \propto \frac{\partial B_\phi^2}{\partial \theta}$
$B_\phi < 0$
$B_\phi = 0$
$B_\phi > 0$

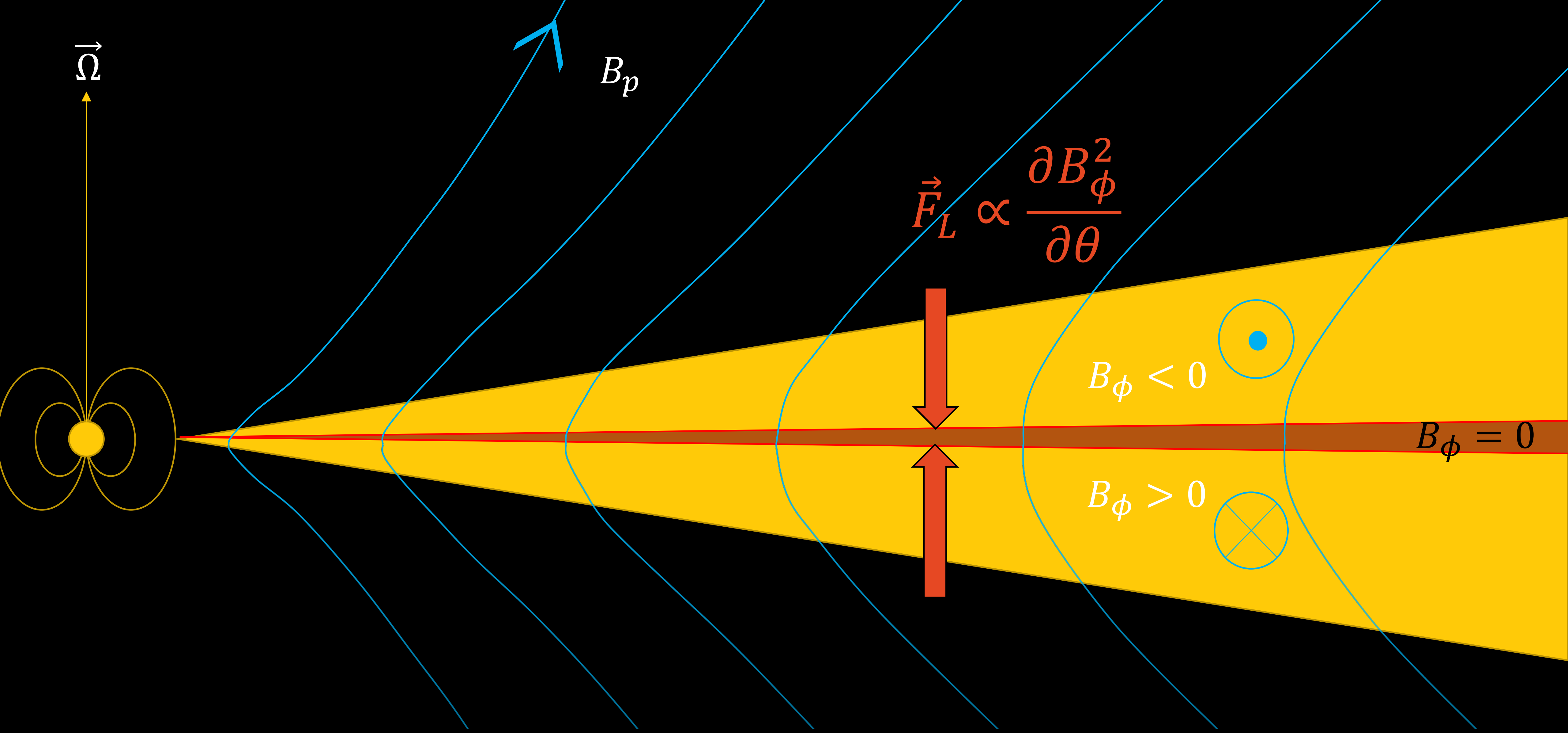

--> Ambipolar diffusion tends to steepen the magnetic gradient at the magnetic null

Brandenburg & Zweibel 1994

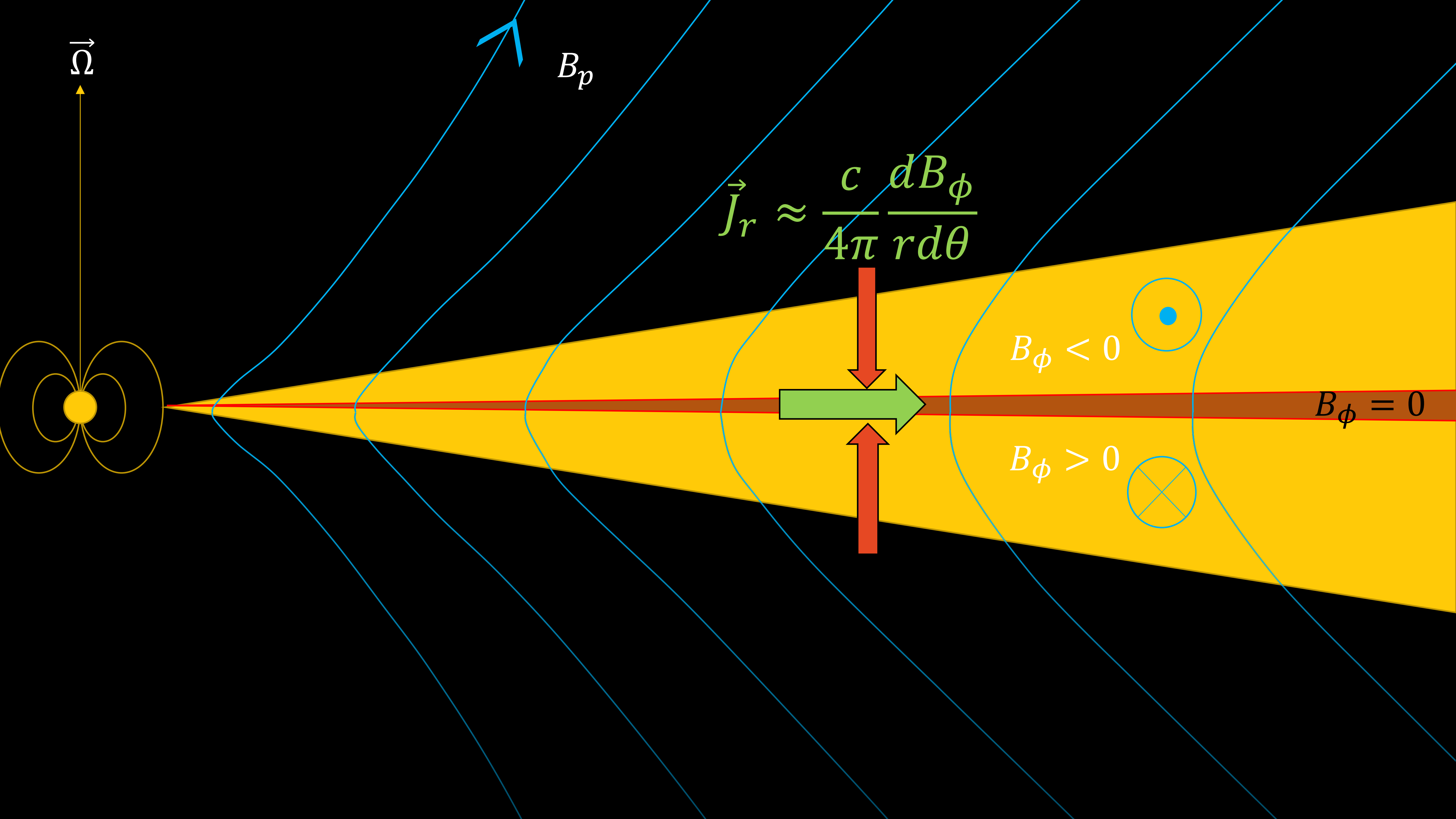

$\vec{\Omega}$
B_p
$\vec{J}_r \approx \frac{c}{4\pi}\frac{dB_\phi}{r d\theta}$
$B_\phi < 0$
$B_\phi = 0$
$B_\phi > 0$

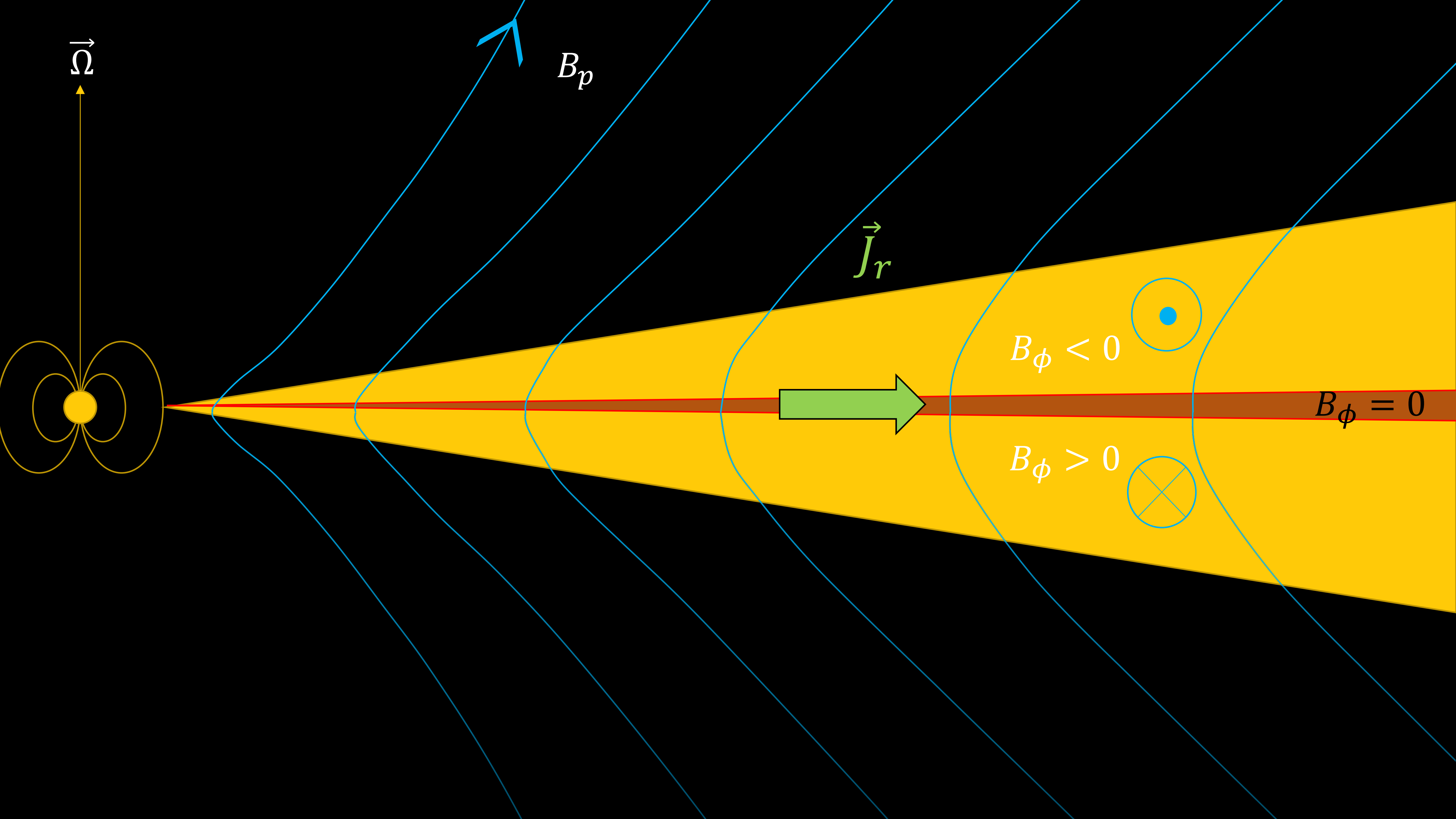

$\vec{\Omega}$
B_p
$\vec{J}_r$
$B_\phi < 0$
$B_\phi = 0$
$B_\phi > 0$

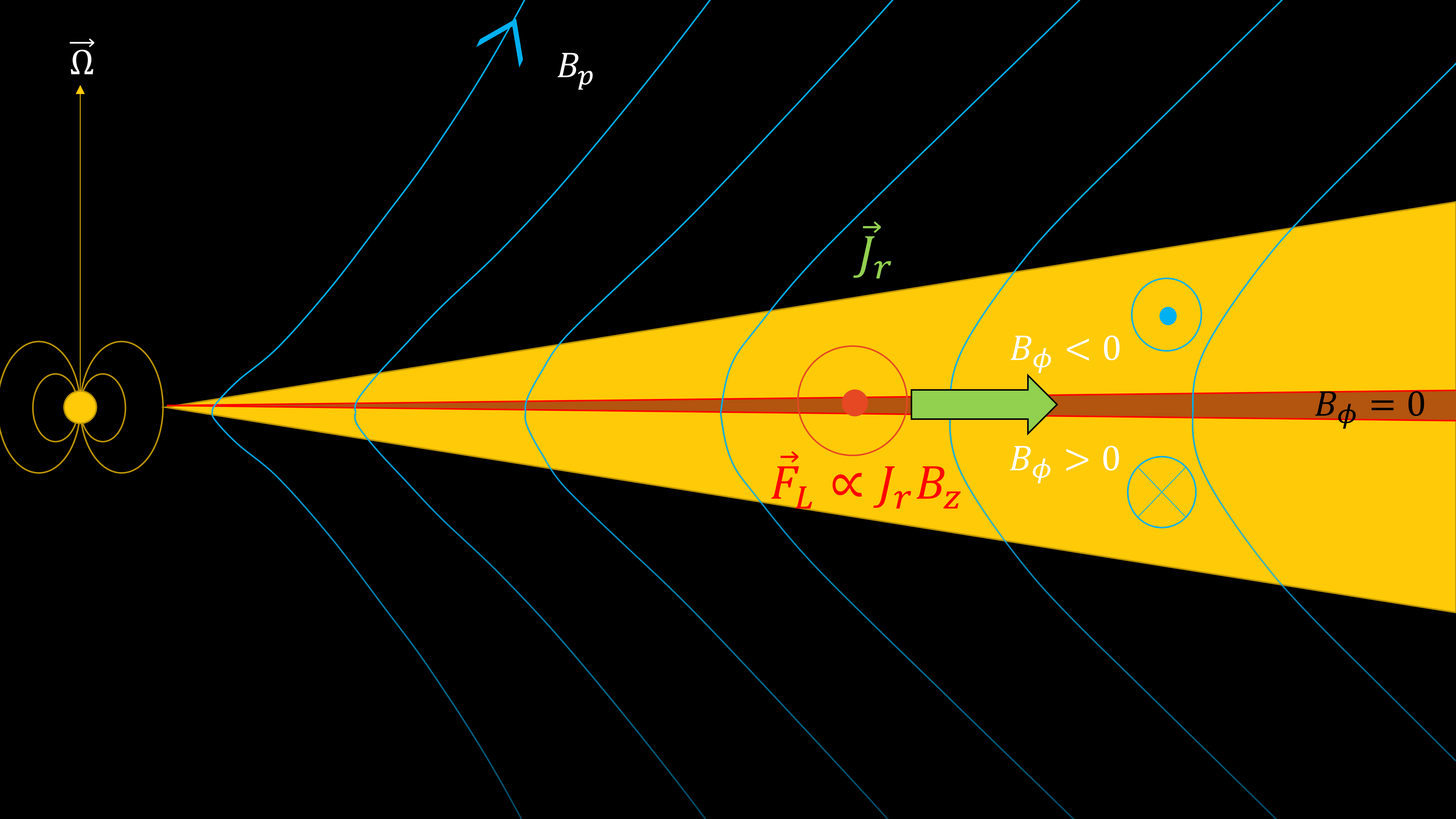

$\vec{\Omega}$
B_p
$\vec{J}_r$
$B_\phi < 0$
$B_\phi = 0$
$B_\phi > 0$
$\vec{F}_L \propto J_r B_z$

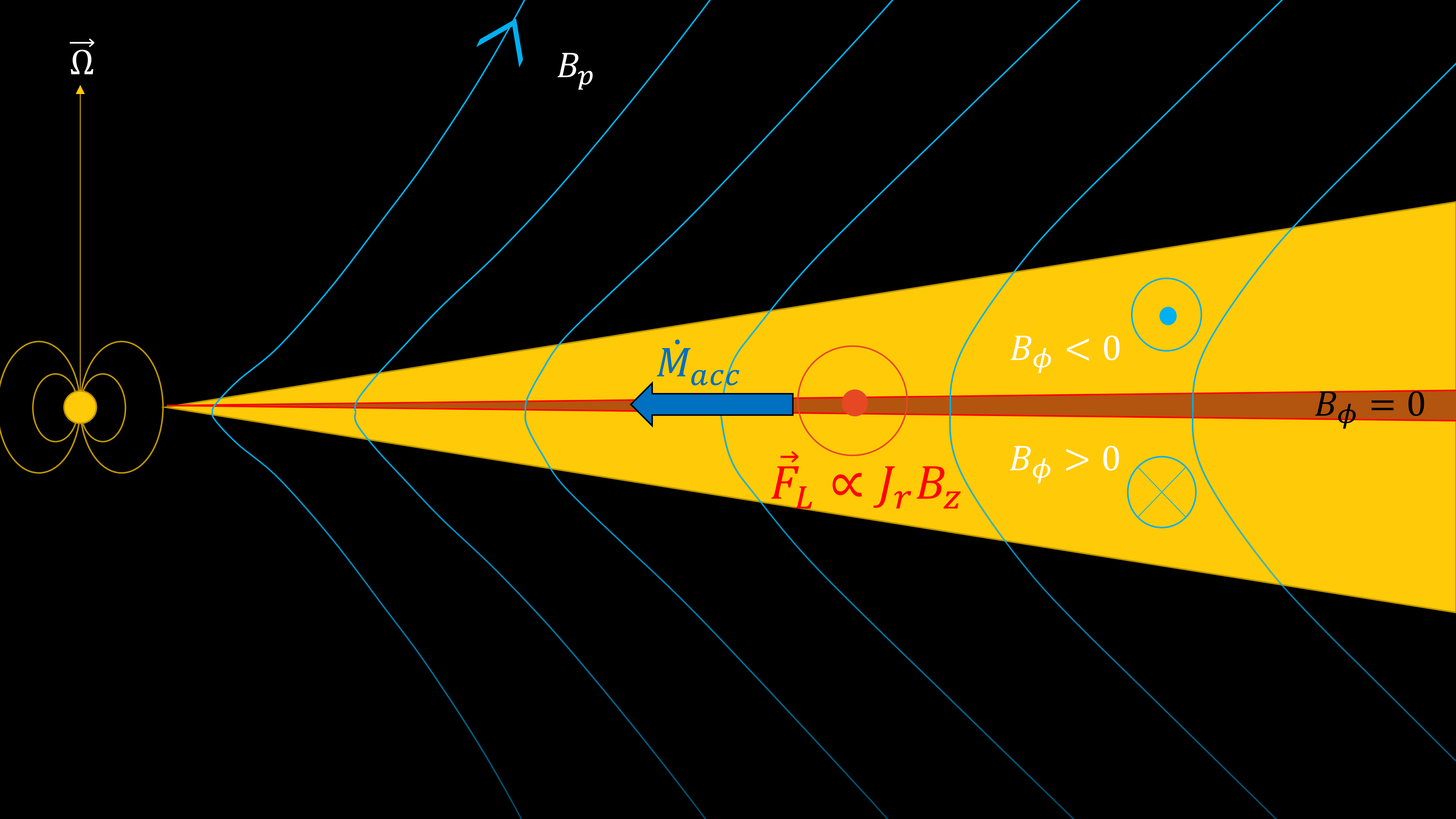

$\vec{\Omega}$
B_p
$\dot{M}_{acc}$
$B_\phi < 0$
$B_\phi = 0$
$B_\phi > 0$
$\vec{F}_L \propto J_r B_z$

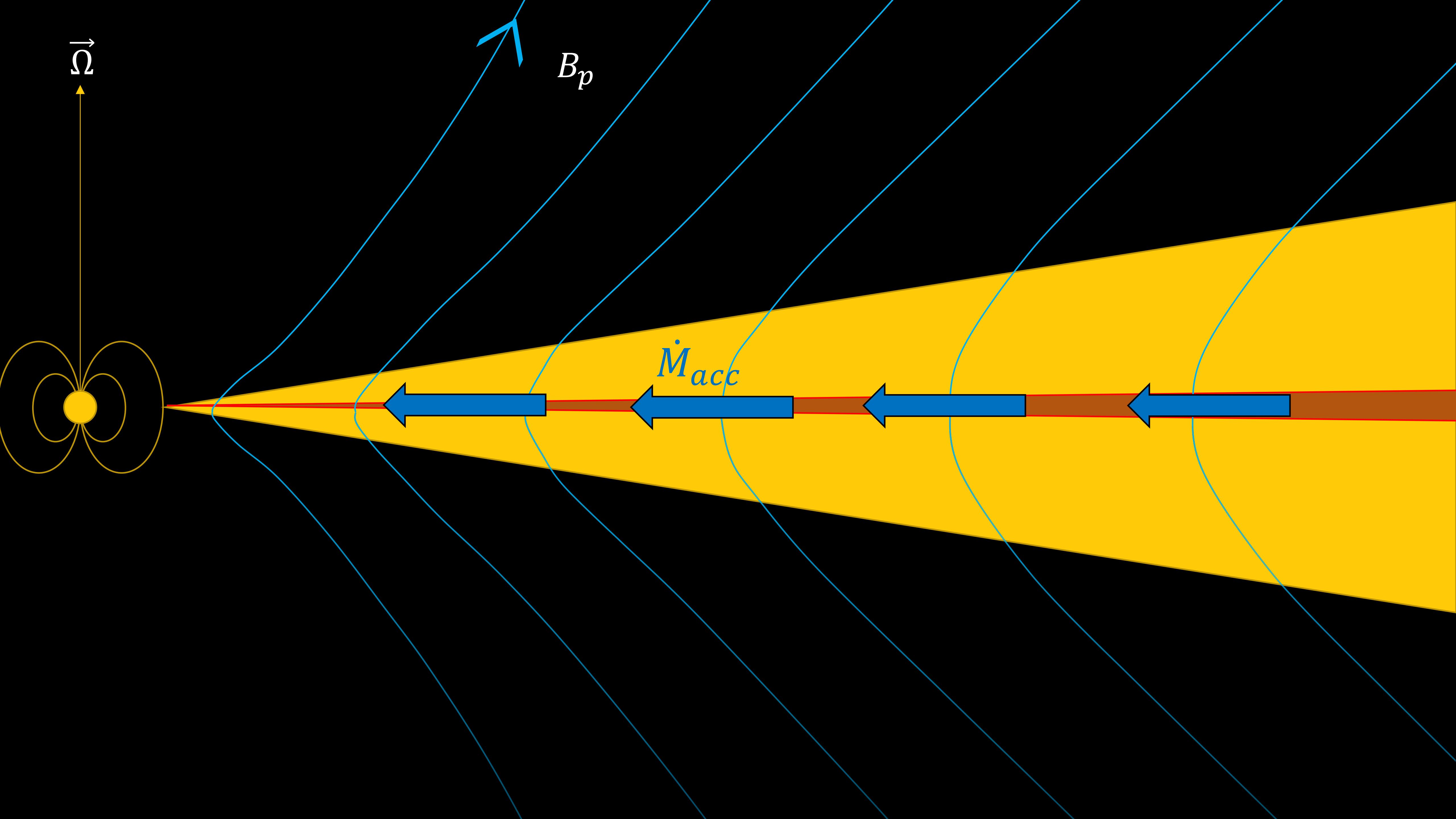
$\vec{\Omega}$
B_p
$\dot{M}_{acc}$

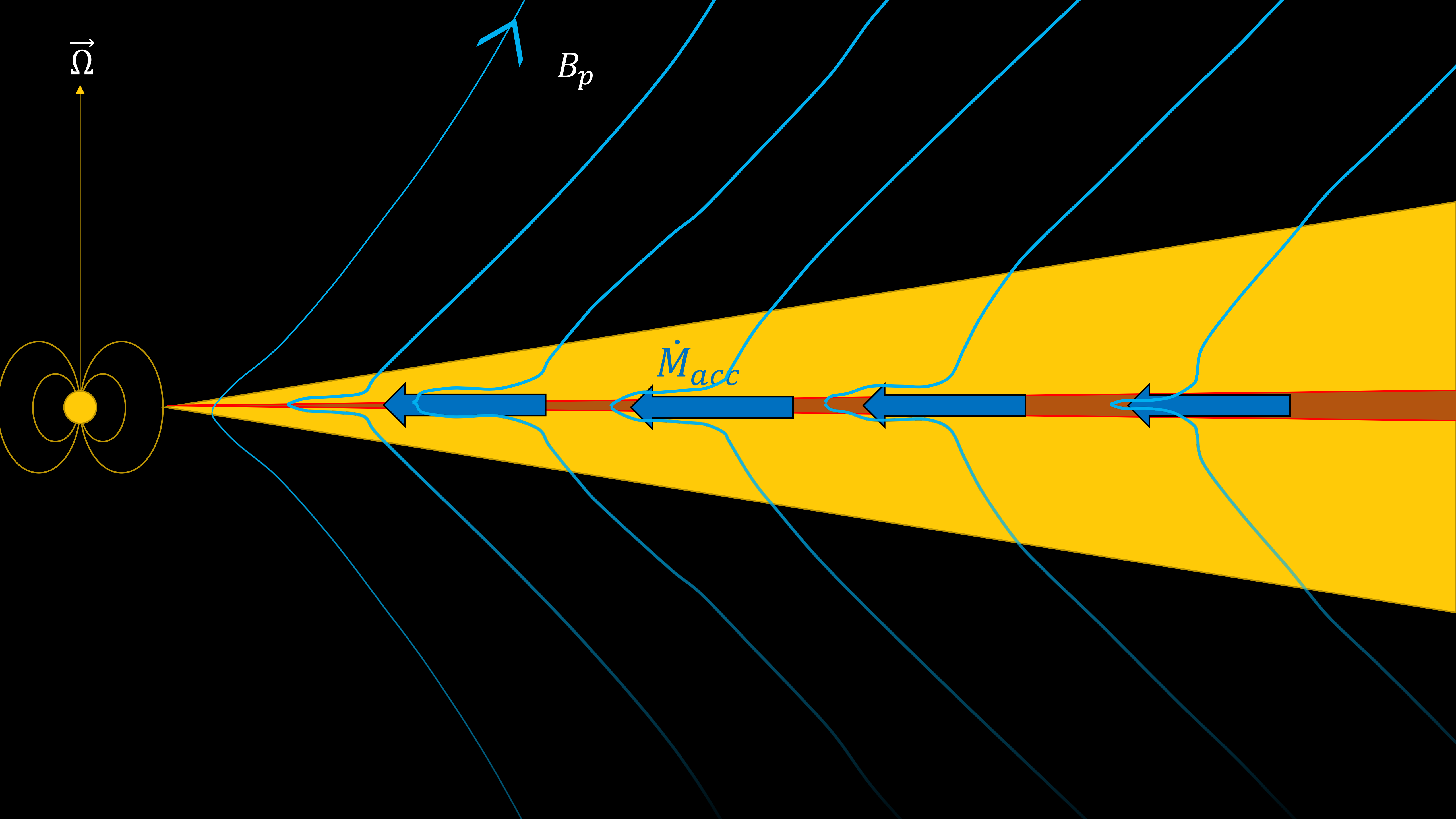

$\vec{\Omega}$
B_p
$\dot{M}_{acc}$

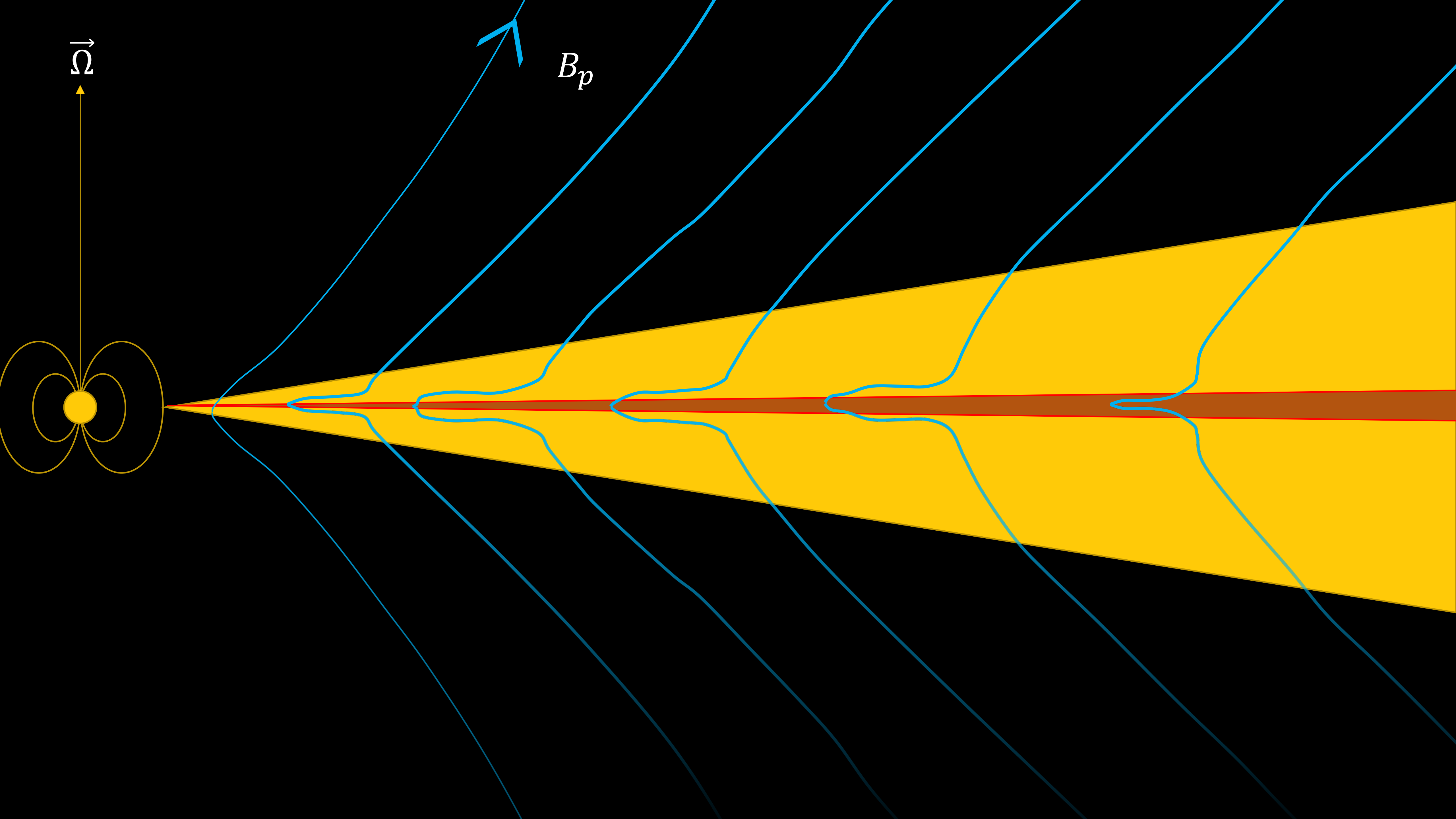

$\vec{\Omega}$
B_p

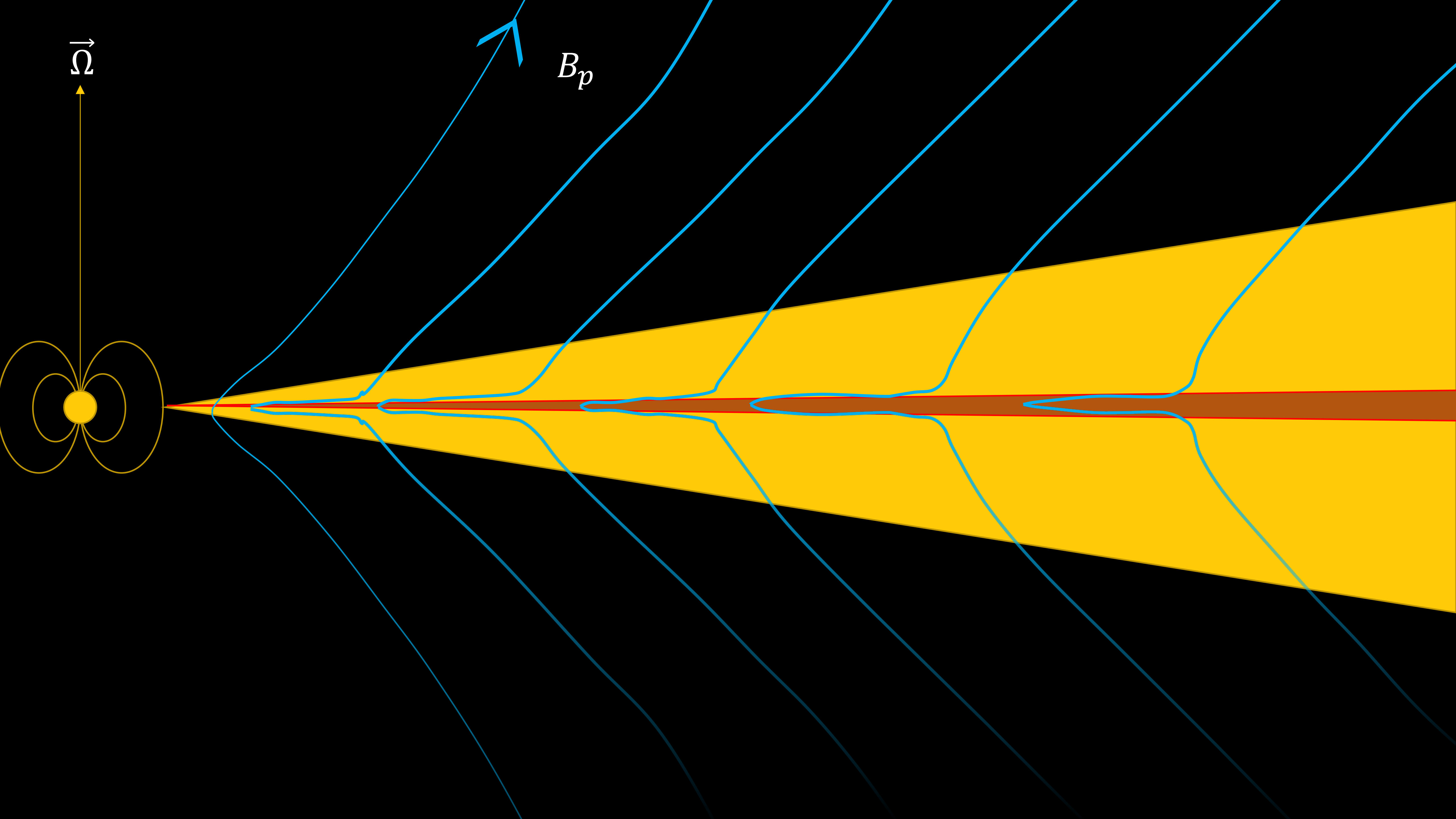
$\vec{\Omega}$
B_p

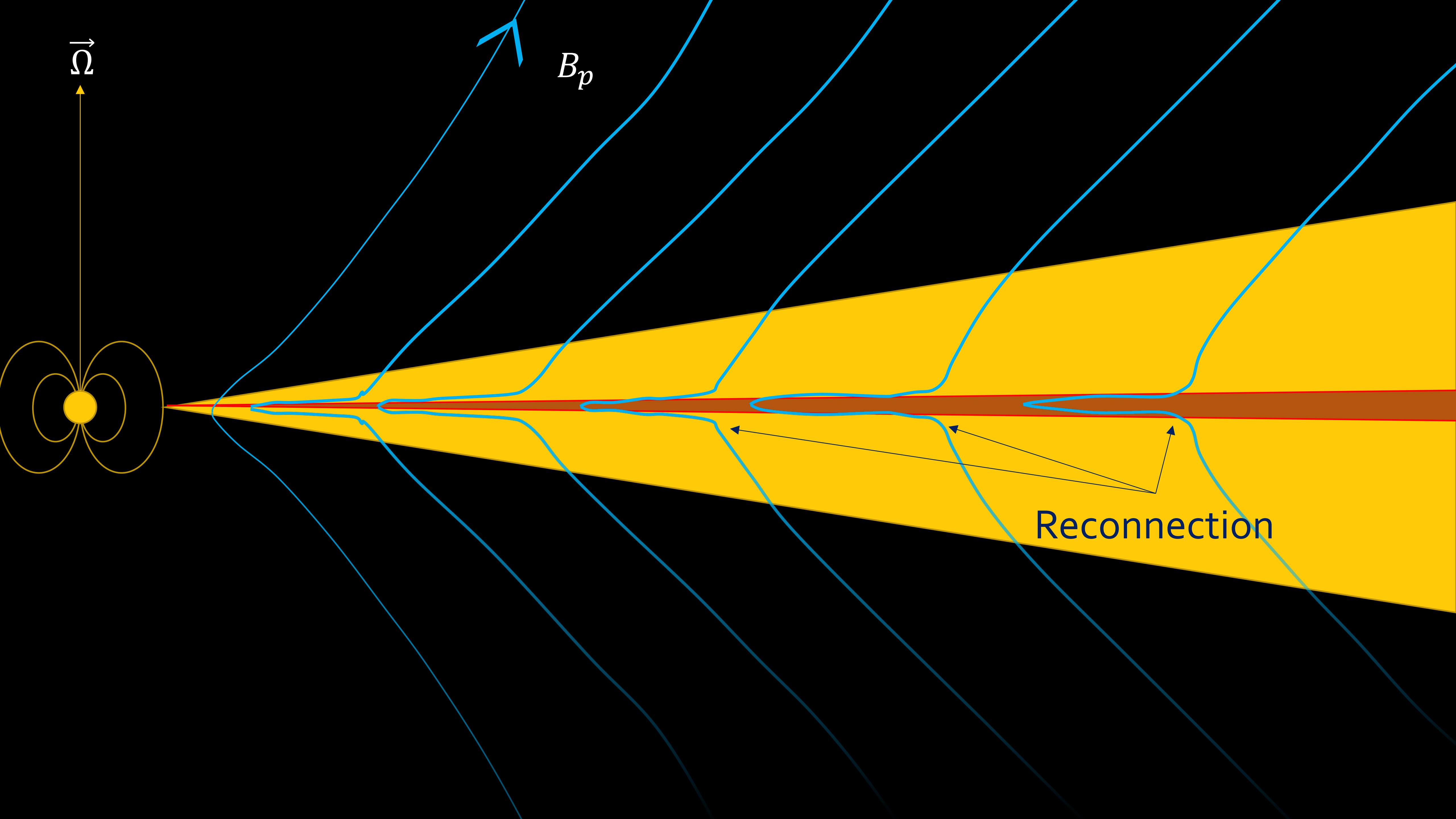

$\vec{\Omega}$
B_p
Reconnection

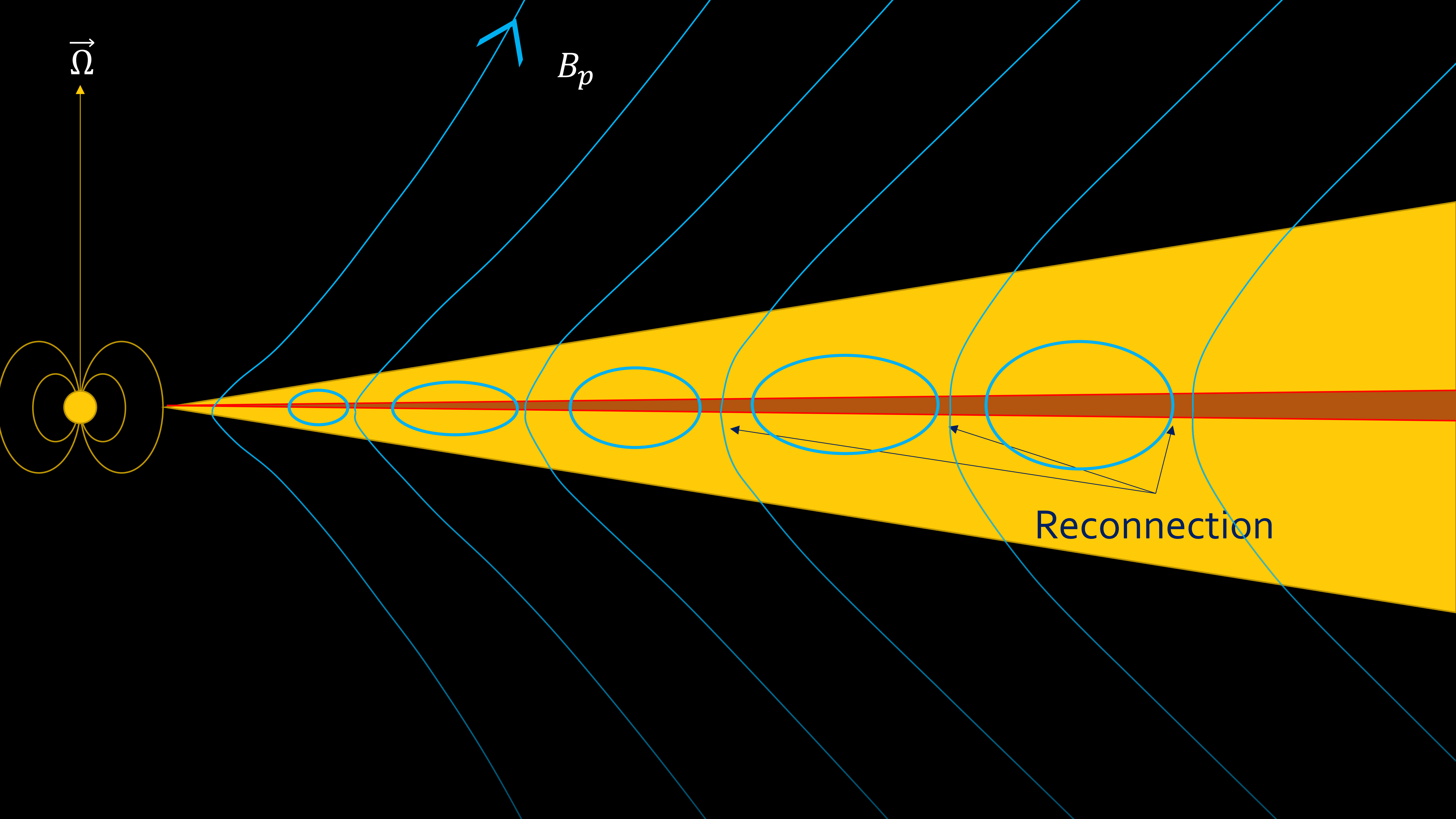

$\vec{\Omega}$
B_p
Reconnection

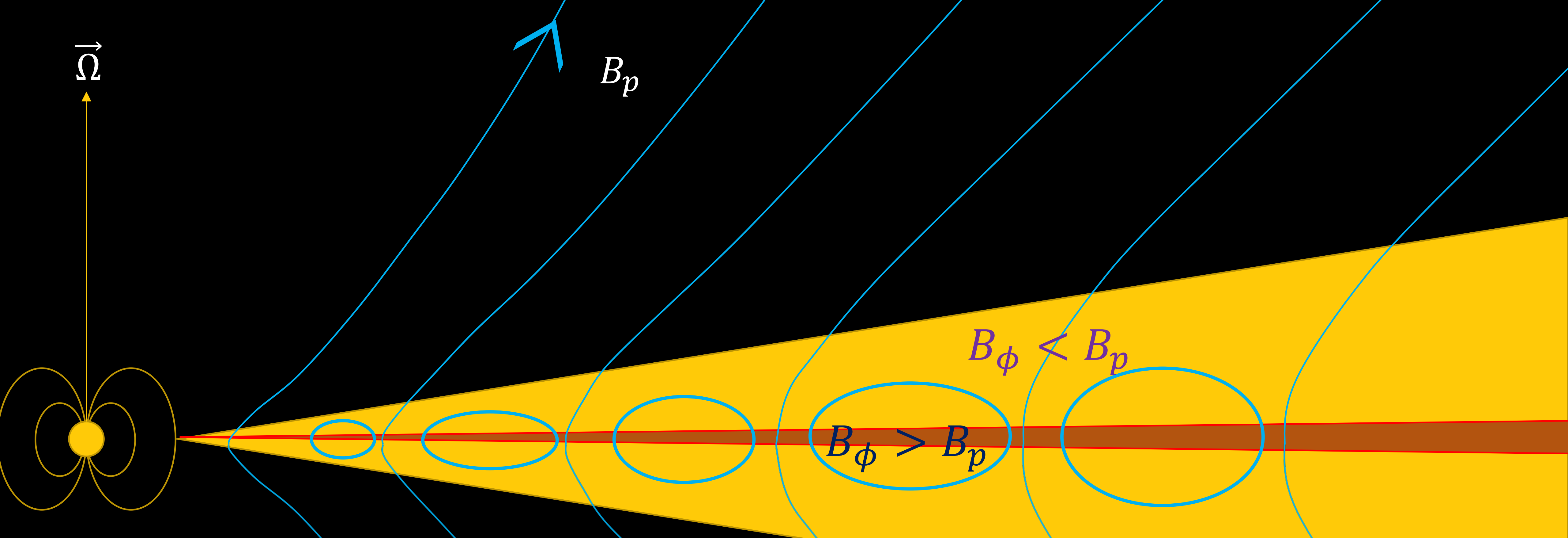

→ To open gap, angular momentum removal rate (or mass accretion rate) must vary as a function of disk radius!

$$\dot{M} \approx \left(\frac{R^2 B_\phi B_\theta}{v_K} \right)$$

Mass accretion rate if angular momentum removal is due to magnetic torque acting on the disk

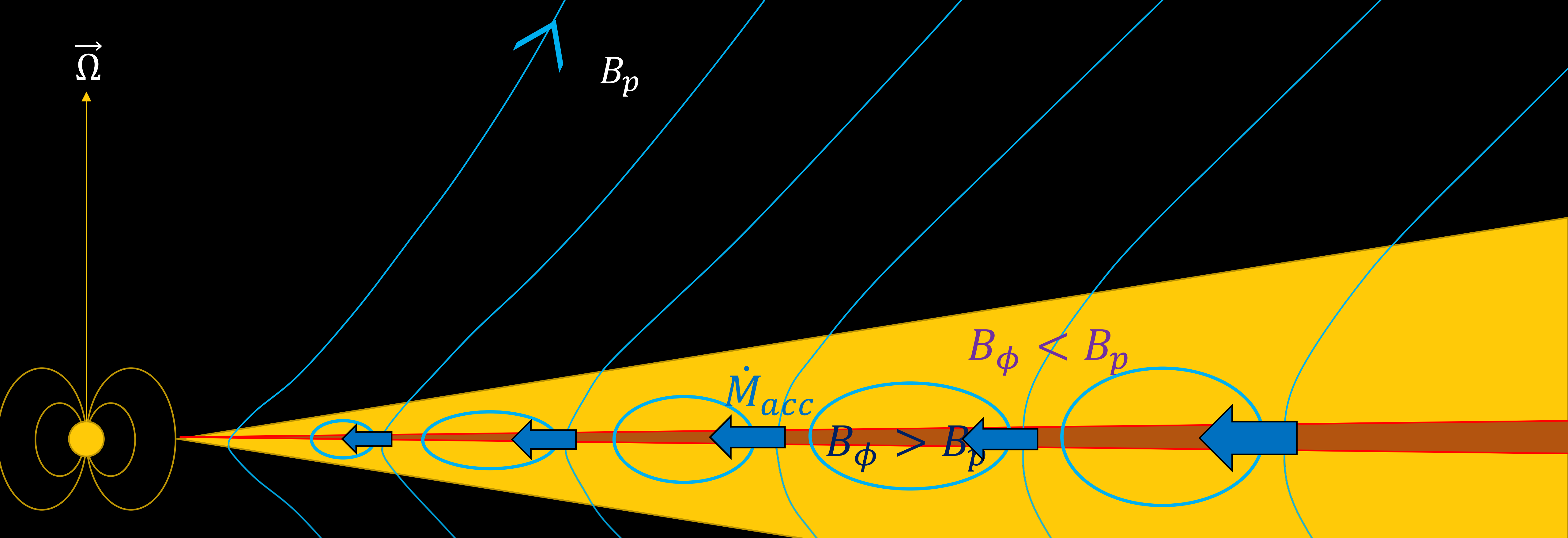

→ To open gap, angular momentum removal rate (or mass accretion rate) must vary as a function of disk radius!

$$\dot{M} \approx \left(\frac{R^2 B_\phi B_\theta}{v_K} \right)$$

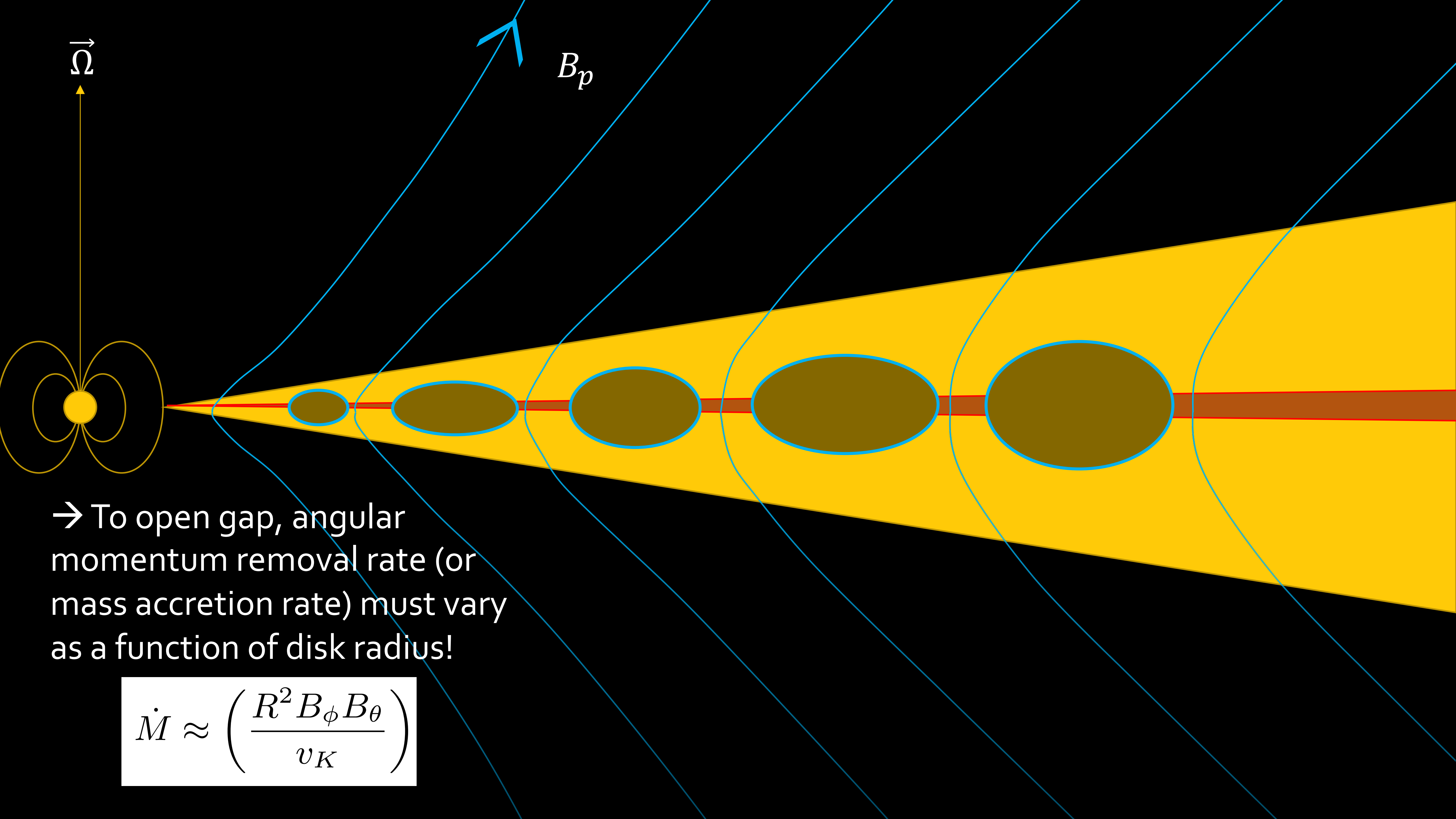

→ To open gap, angular momentum removal rate (or mass accretion rate) must vary as a function of disk radius!

$$\dot{M} \approx \left(\frac{R^2 B_\phi B_\theta}{v_K} \right)$$

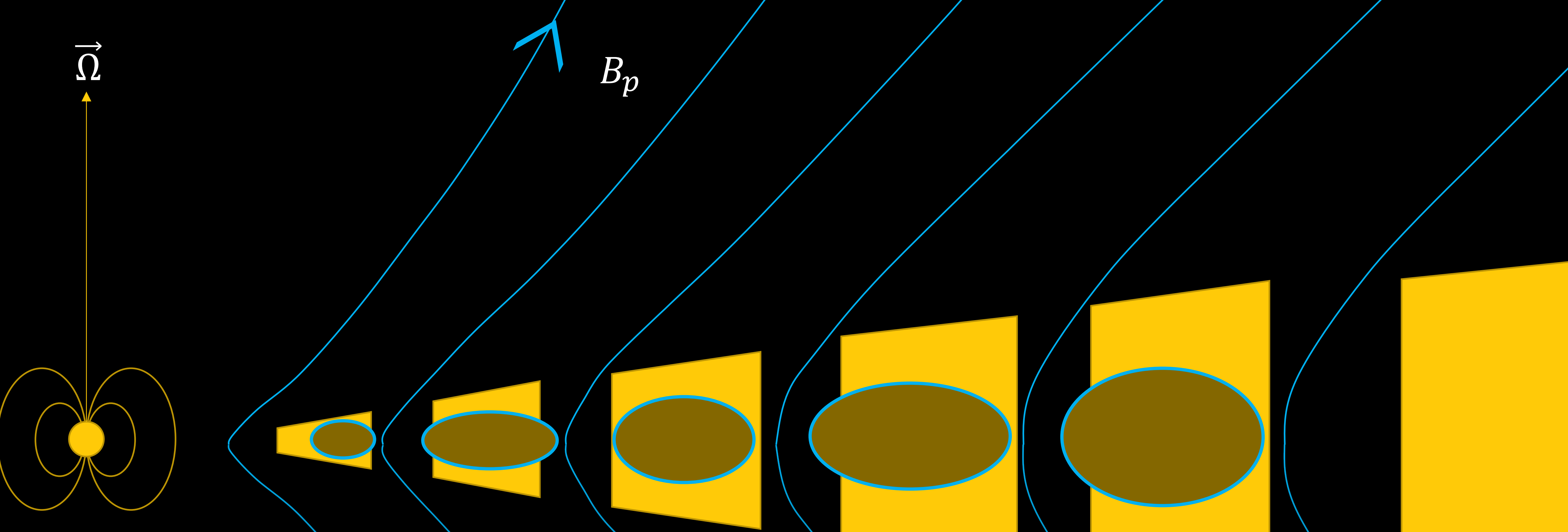

→ To open gap, angular momentum removal rate (or mass accretion rate) must vary as a function of disk radius!

$$\dot{M} \approx \left(\frac{R^2 B_\phi B_\theta}{v_K}\right)$$

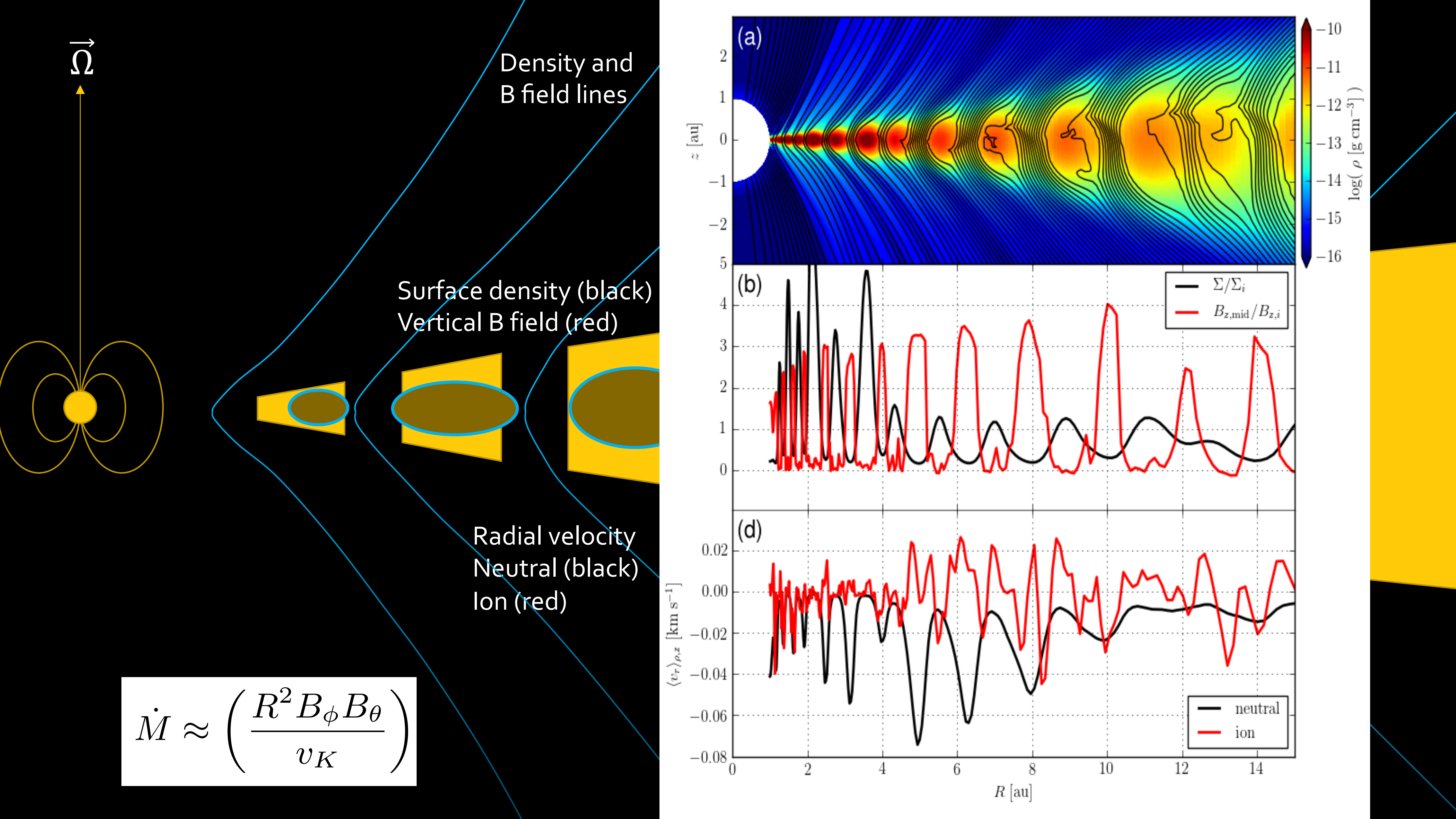

$\vec{\Omega}$
Density and
B field lines
Surface density (black)
Vertical B field (red)
Radial velocity
Neutral (black)
Ion (red)
$$\dot{M} \approx \left(\frac{R^2 B_\phi B_\theta}{v_K} \right)$$
(a)
(b)
(d)
z [au]
$\log(\ \rho\ [\mathrm{g\ cm^{-3}}]\ )$
Σ/Σ_i
$B_{z,\mathrm{mid}}/B_{z,i}$
$\langle v_r \rangle_{\rho,z}$ [km s^{-1}]
neutral
ion
R [au]

3D Simulation setup

- Axisymmetric (includes phi vector components)
- Non-rotating, hydrostatic corona above disk with pressure balanced at disk surface
- Two hemispheres
- Ambipolar diffusion with $\rho_{ion} \propto \rho^{1/2}$ with transition to ideal MHD above initial disk surface
- ***Three dimensions***

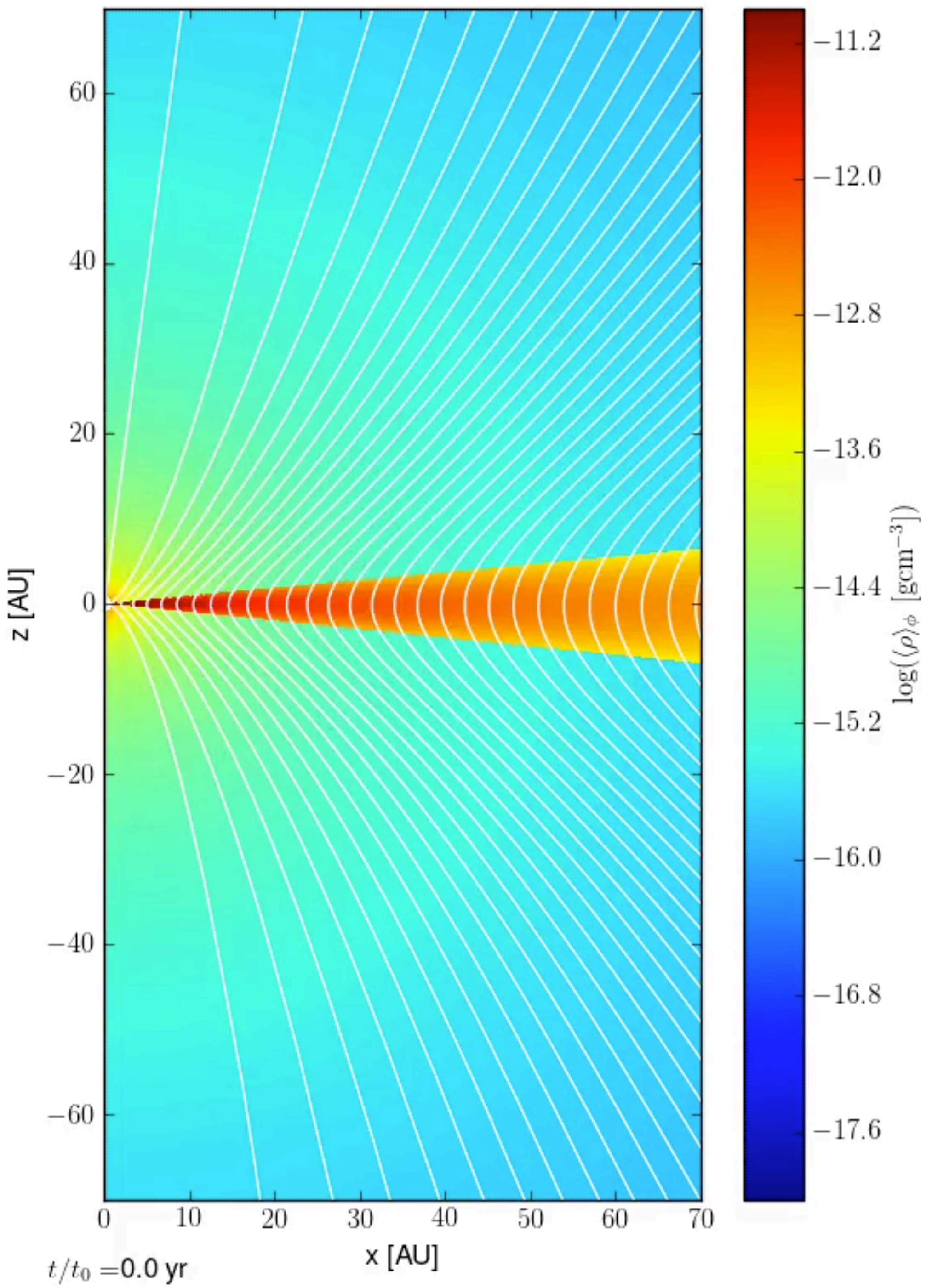

3D

- Axisy
- Non-r
  press
- Two h
- Ambi
  to ide
- ***Thi***

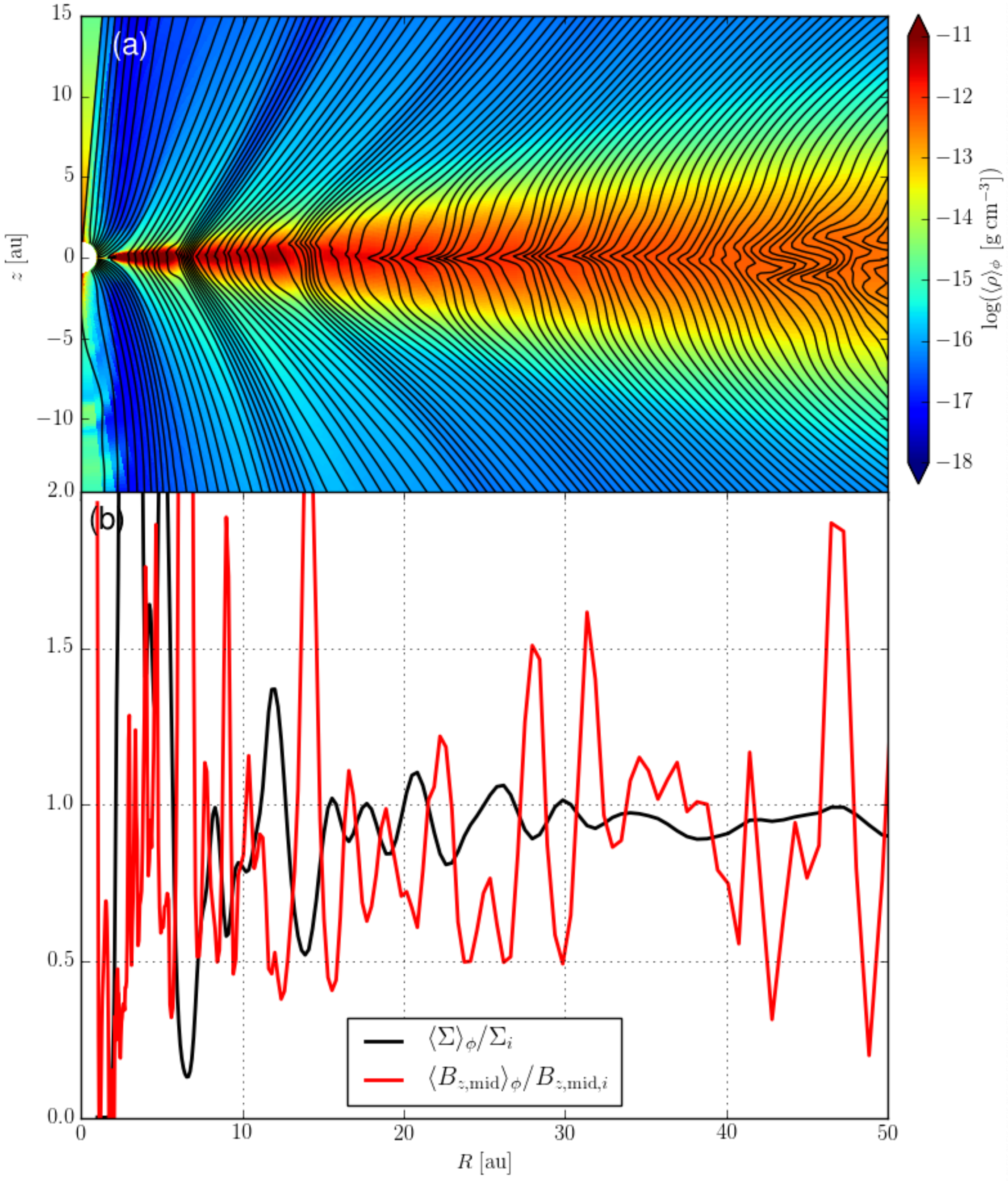

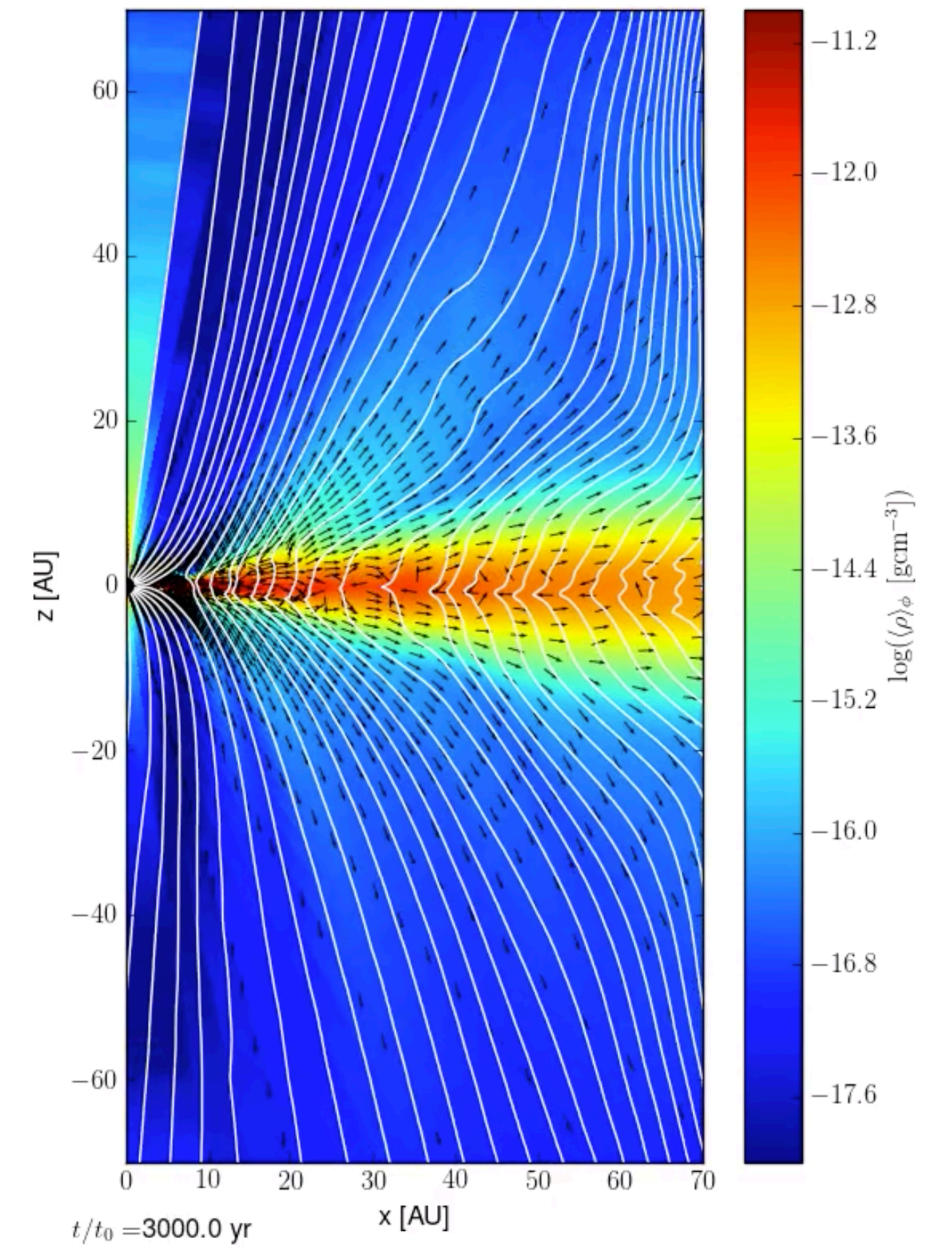

Surface density

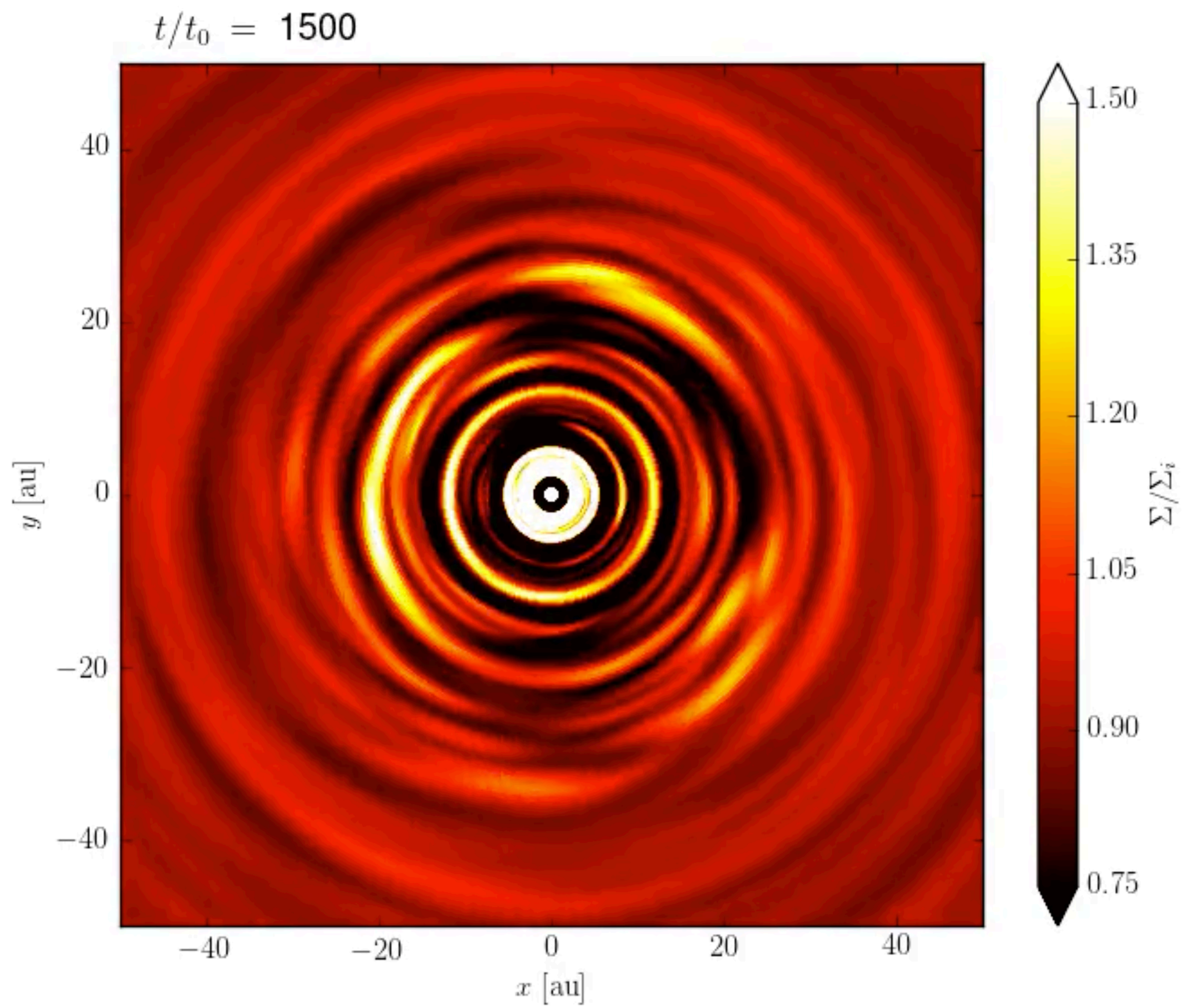

Vertical magnetic field at midplane

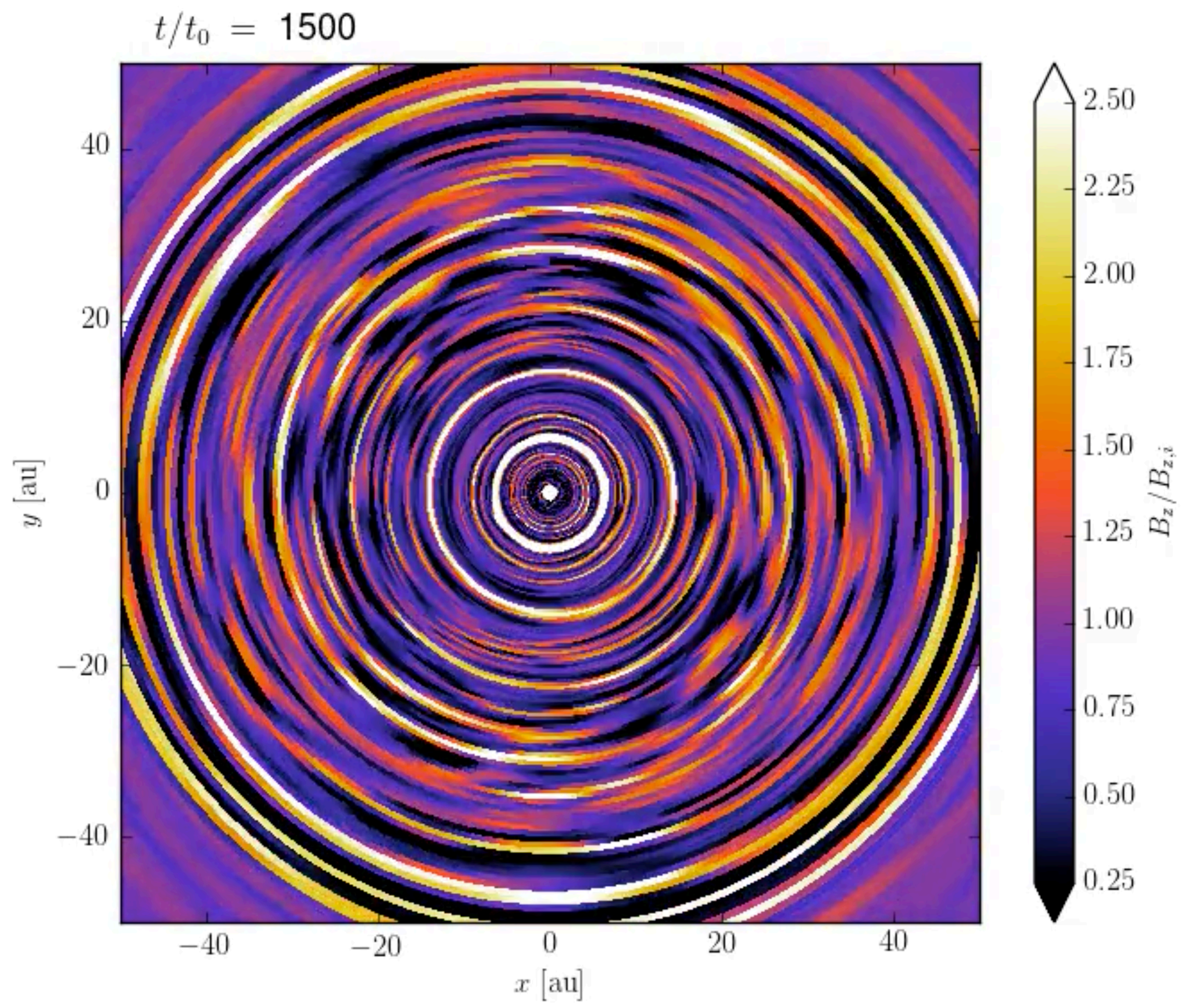

Ring spacing from magnetic reconnection

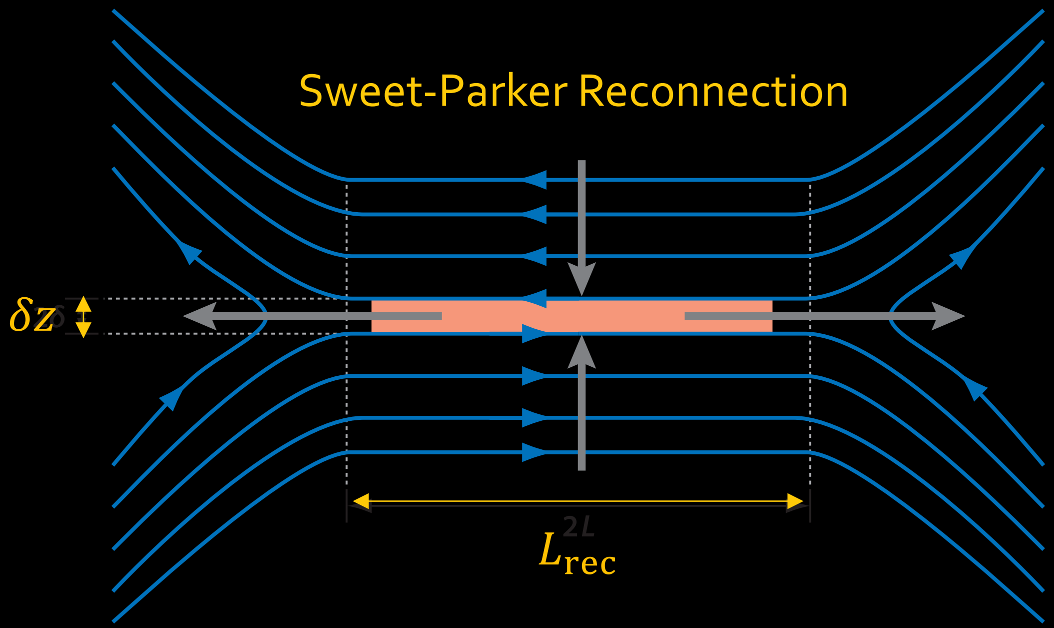

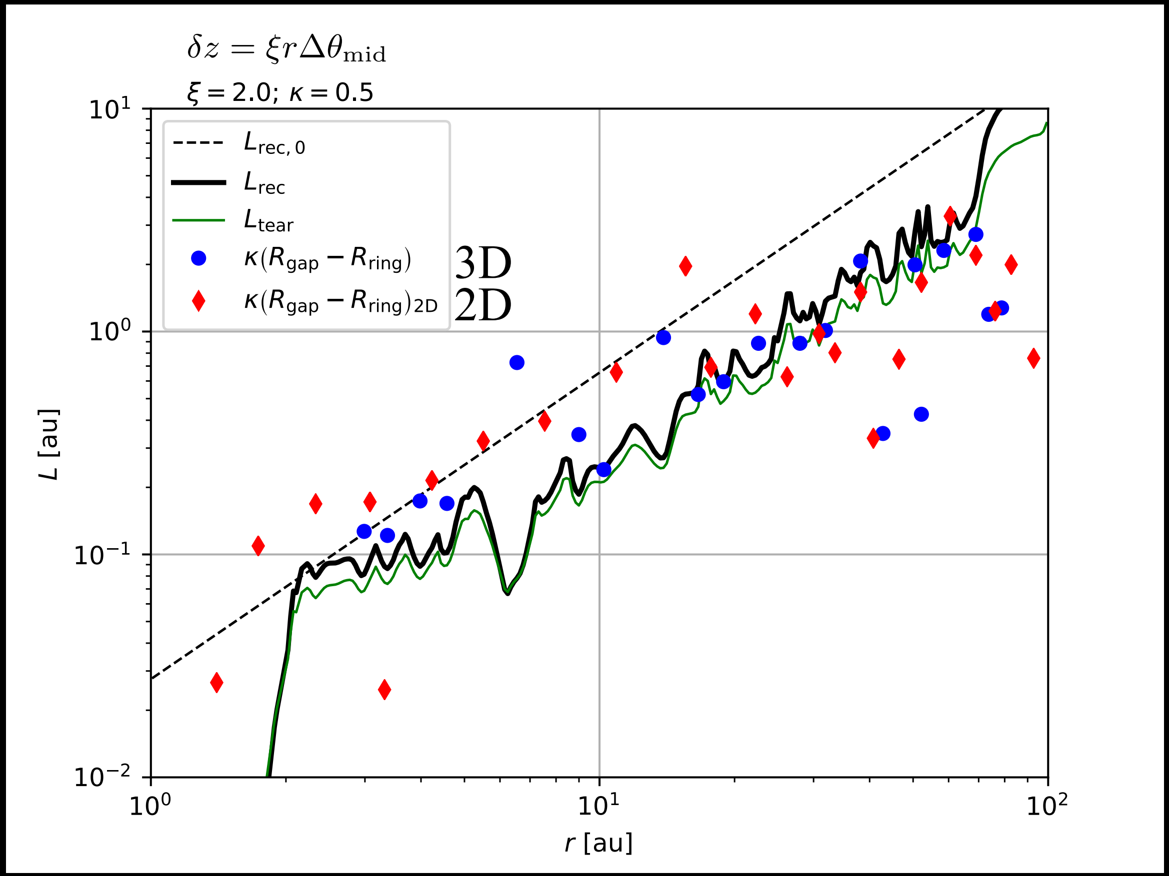

$$\frac{\delta z}{L_{\rm rec}} = S^{-1/2}; \quad S = \frac{h v_A}{\eta_A}$$

Zweibel+Yamada 2009

Which grains are launched in the wind?

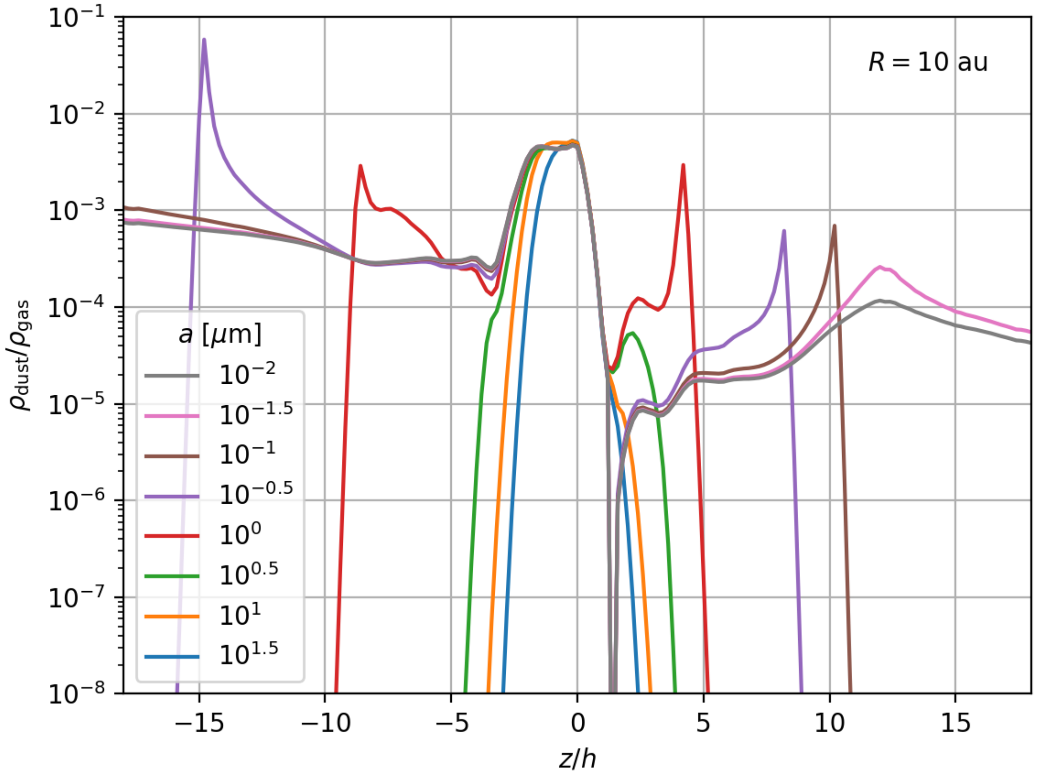

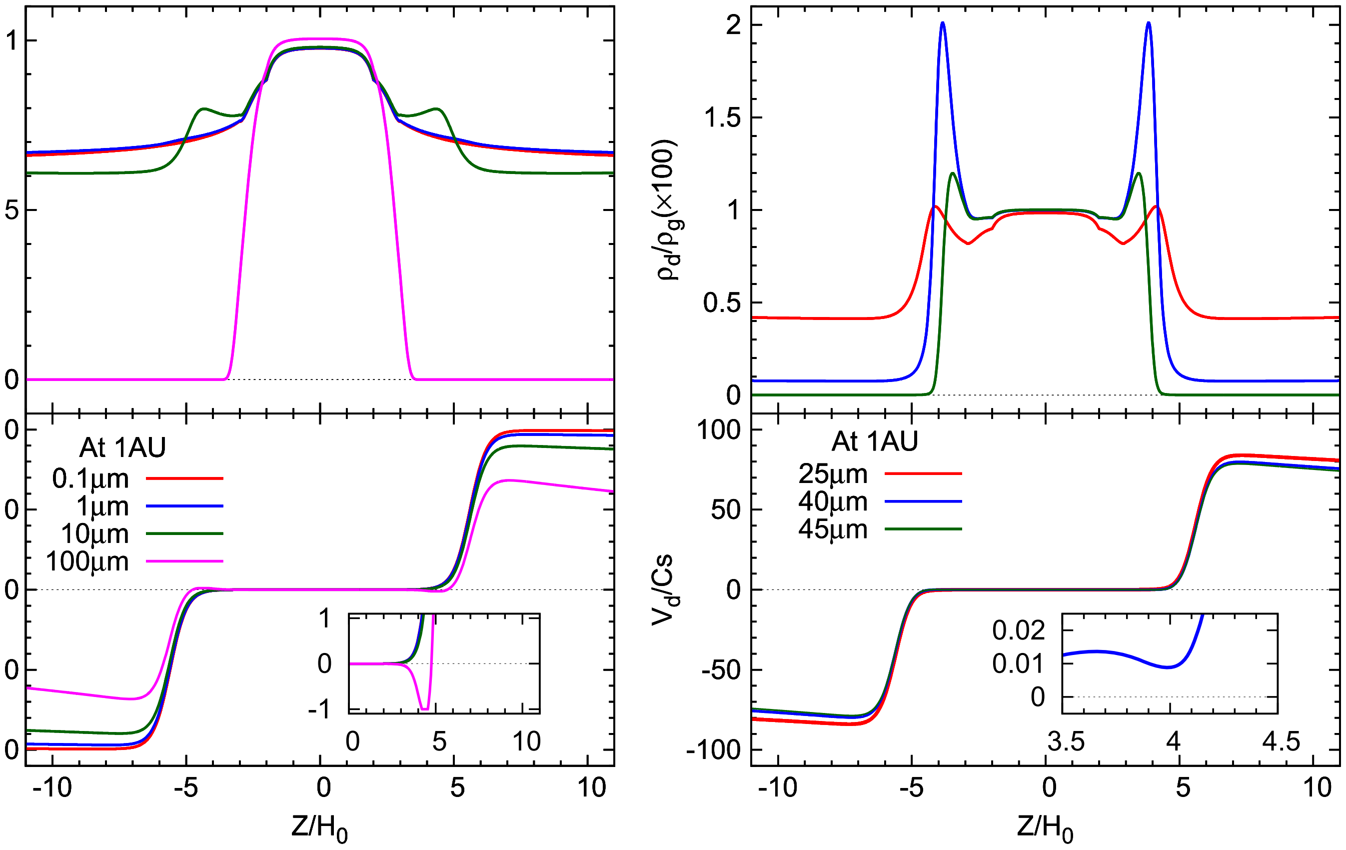

Miyake+ 16
(see also Riols + Lesur 18)

Obscuration by dusty disk wind

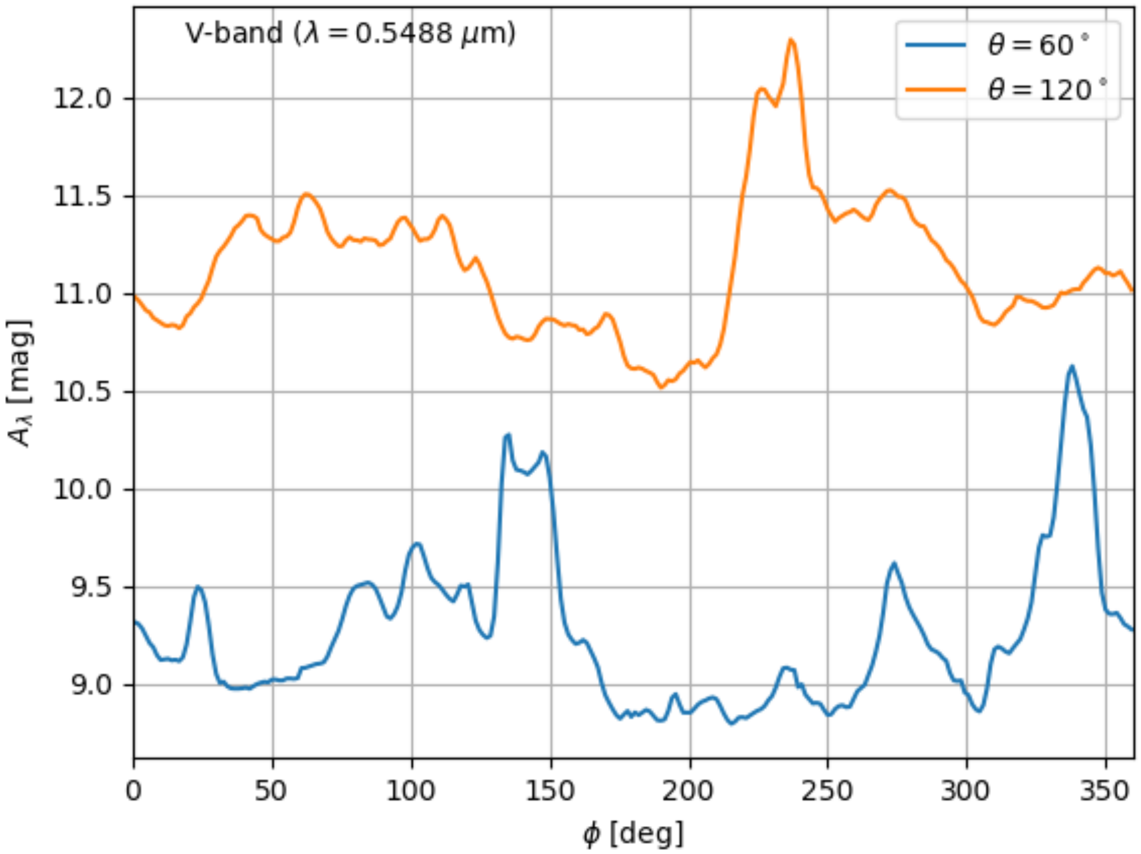

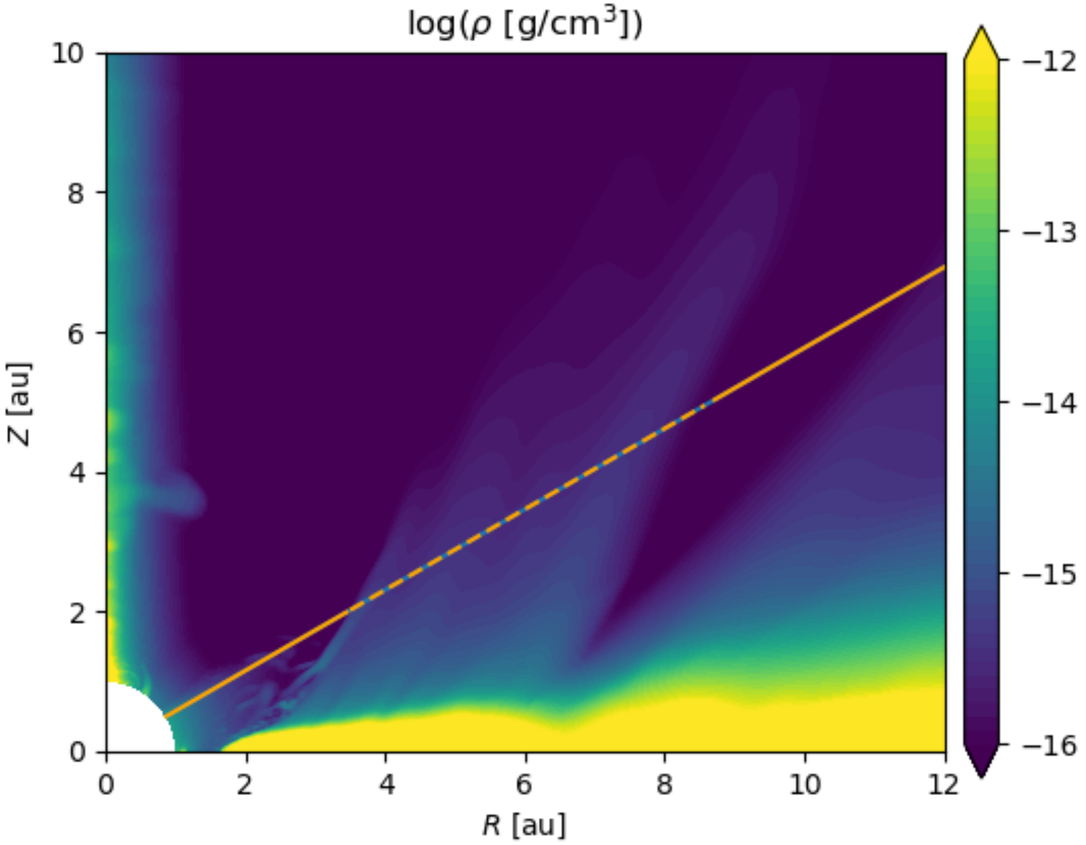

Obscuration by dusty disk wind

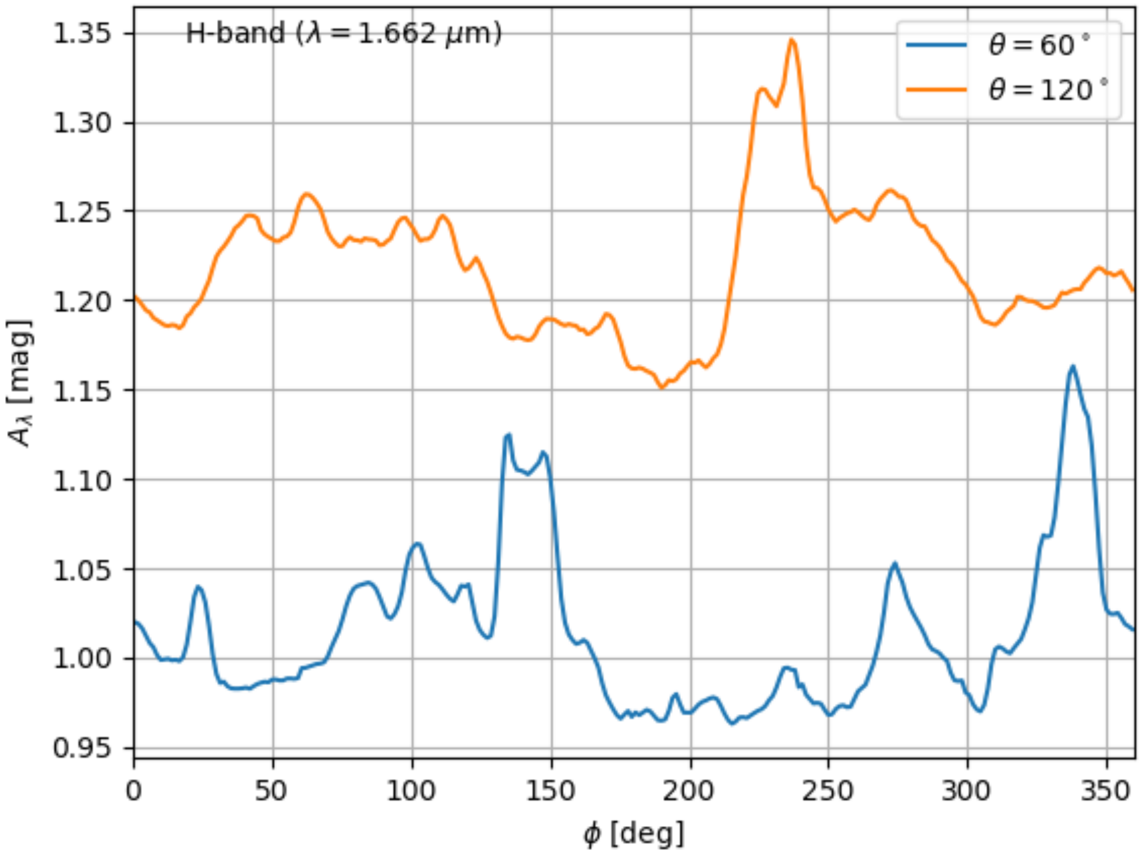

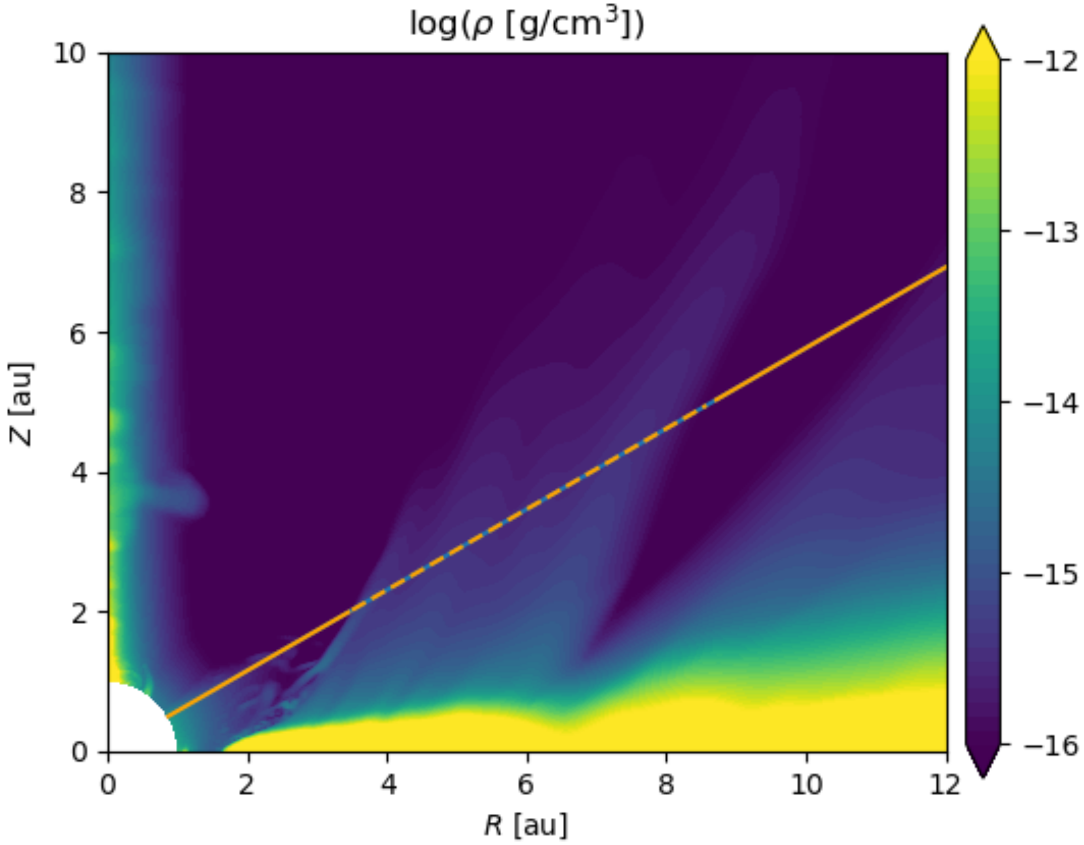

Obscuration by disk winds

Optical fading and NIR brightening events

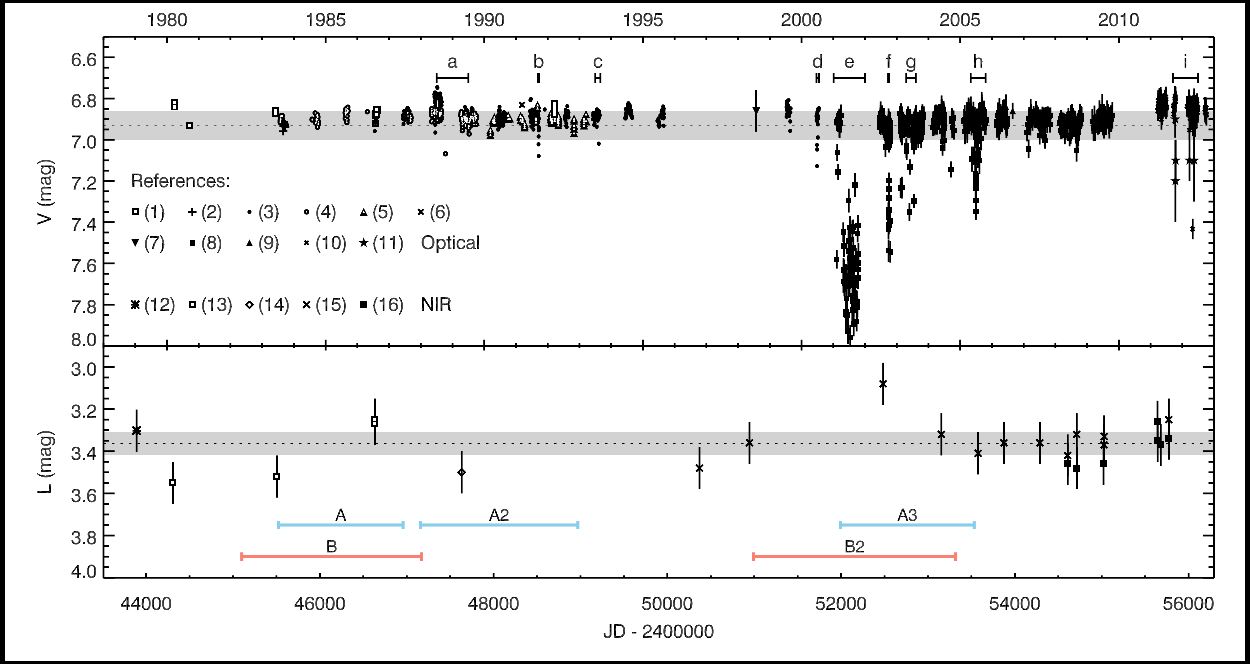

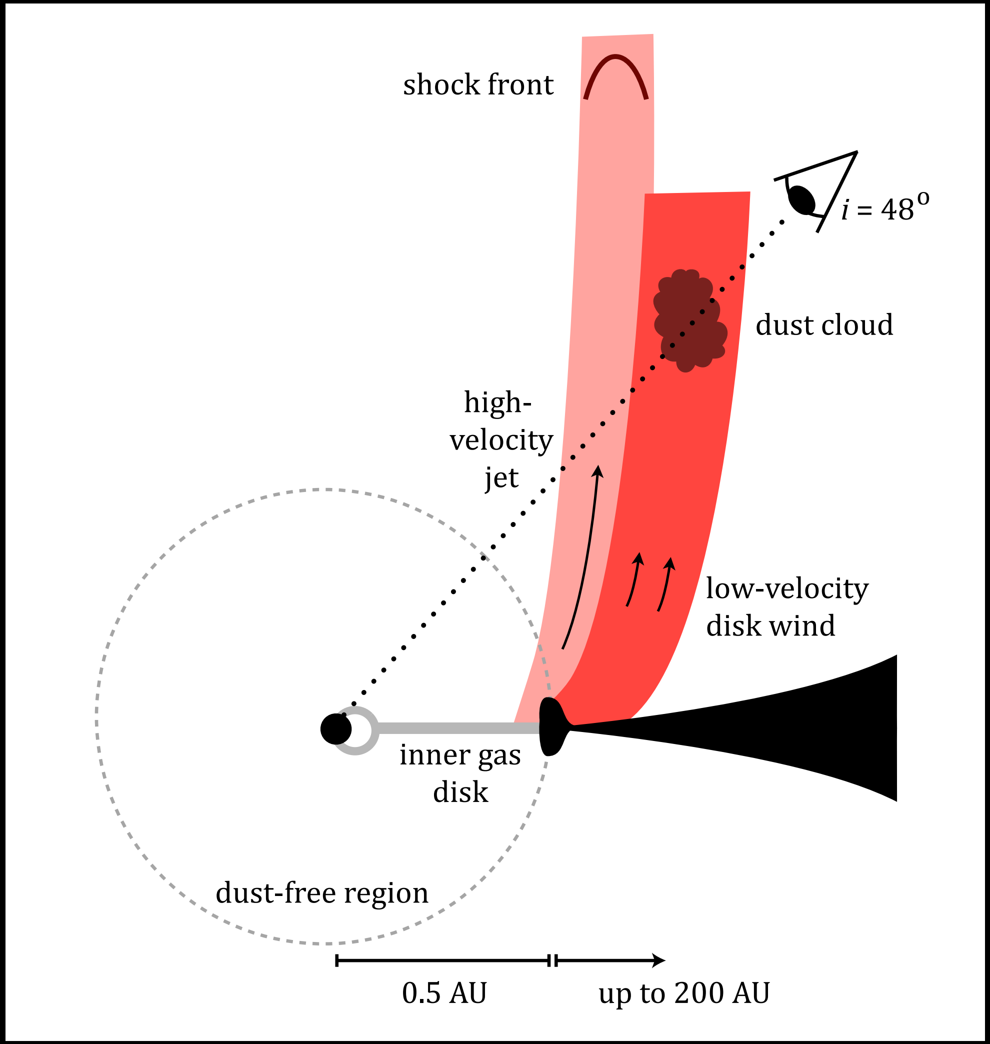

Ellerbroek+ 14

Observational Implications

- RADMC-3D: Three-dimensional Monte-Carlo radiative transfer simulations (Dullemond +2012)

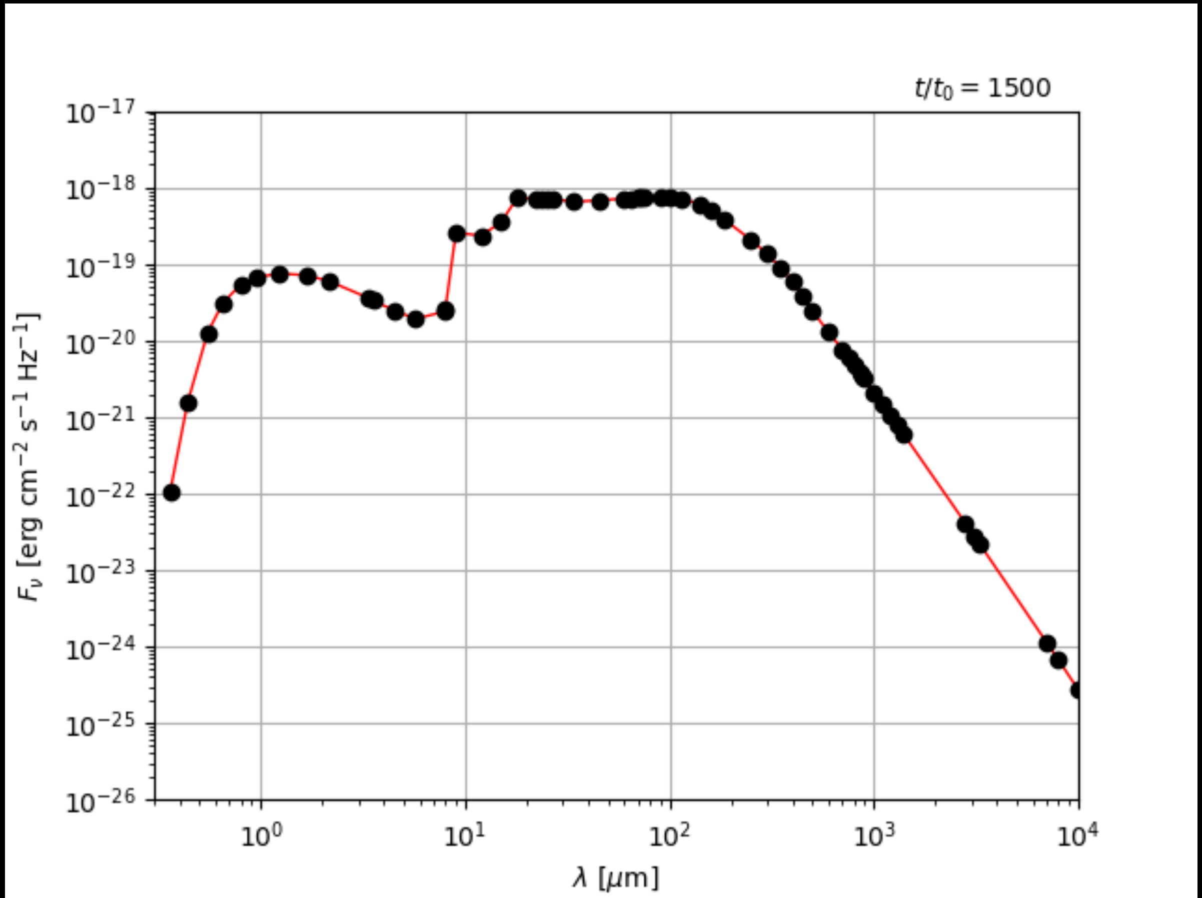

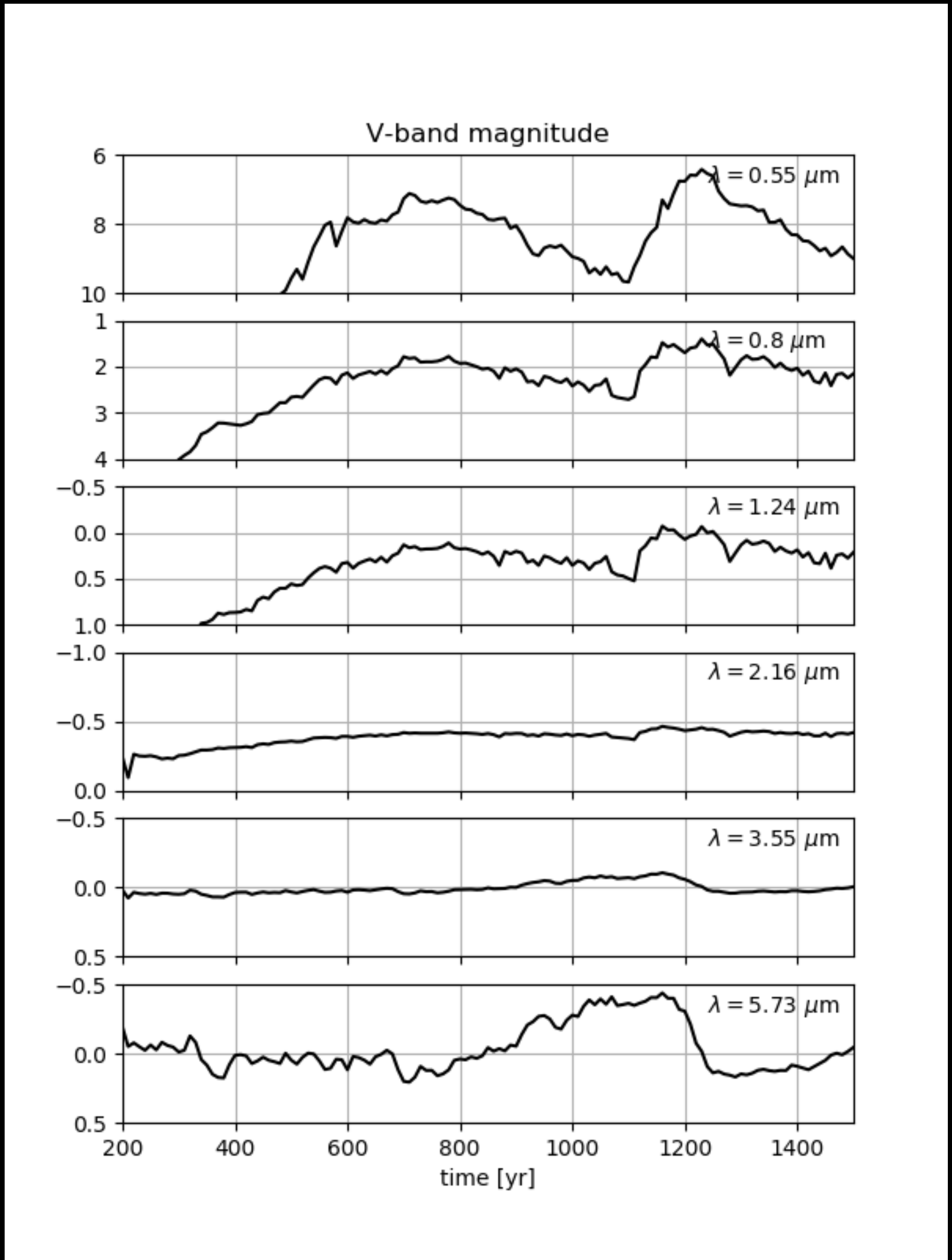

Summary

- The vertical magnetic fields that launch disk winds spontaneously create complex radial substructure over a range of field strengths and diffusivities
- Mechanism for creating disk substructure in AD simulations: Reconnection of pinched radial magnetic field leads to variation of B_Z as a function of radius
- Ring and gap formation is robust in 3D for relatively diffusive disks
- Dusty disk winds from inner rings may explain optical/ NIR variability